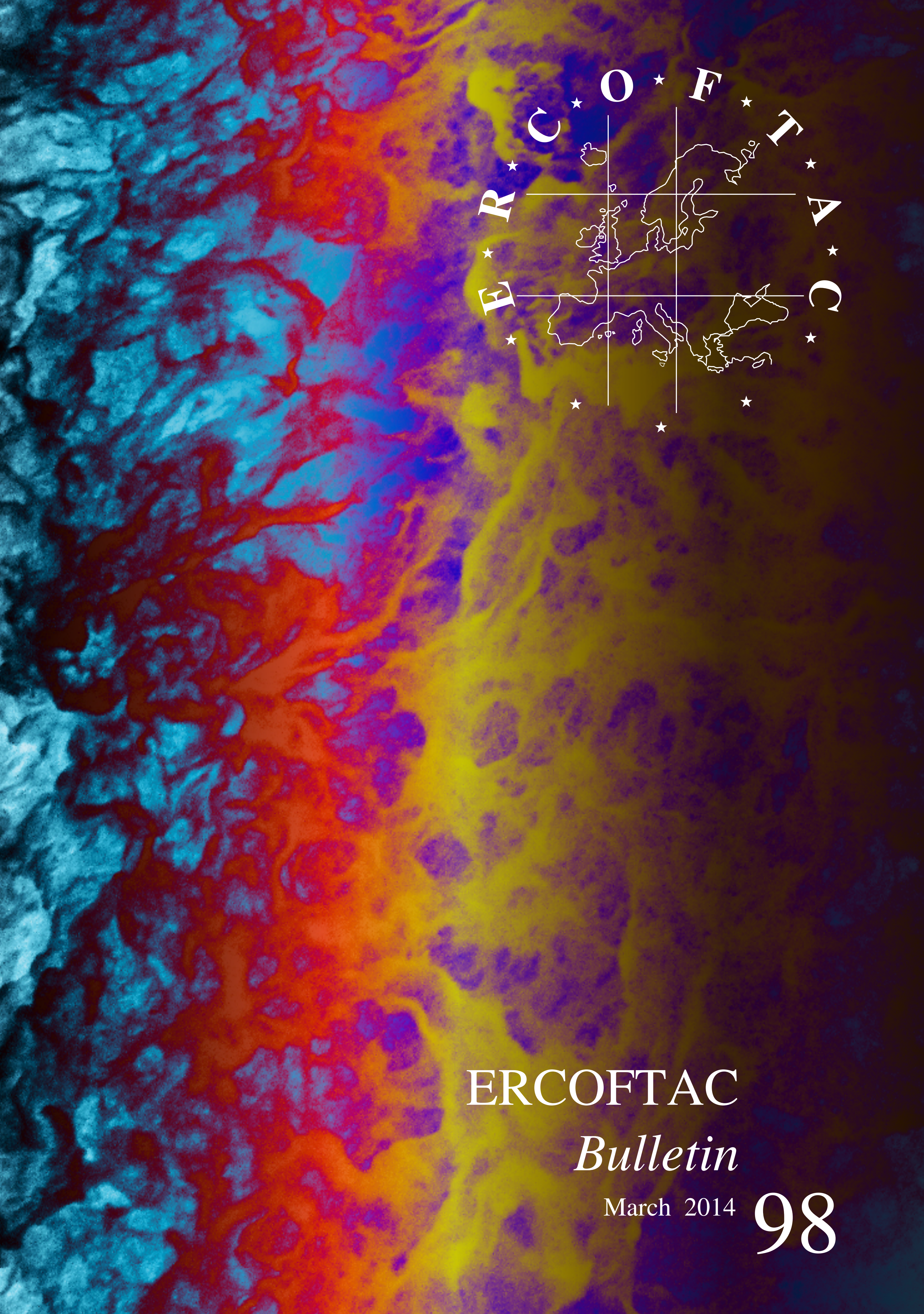

ERCOFTAC

Bulletin

March 2014 98

European Research Community on Flow, Turbulence and Combustion

ERCOFTAC is a leading European association of research, education and industry groups in the technology of flow, turbulence and combustion. The main objectives of *ERCOFTAC* are: To promote joint efforts of European research institutes and industries with the aim of **exchanging technical and scientific information**; to promote **Pilot Centres** for collaboration, stimulation and application of research across Europe; to stimulate, through the creation of **Special Interest Groups**, wellcoordinated European-wide research efforts on specific topics; to stimulate the creation of advanced training activities; and to be influential on funding agencies, governments, the European Commission and the European Parliament.

www.ercoftac.org

Table Of Contents

Submissions

ERCOFTAC Bulletin
Institute of Thermal Machinery
Częstochowa University of Technology
Al. Armii Krajowej 21
42-201 Częstochowa
Poland
Tel: +48 343 250 507
Fax: +48 343 250 507
Email:ercoftac@imc.pcz.czest.pl

Hosted, Printed & Distributed By

Częstochowa University of Technology

Next *ERCOFTAC* Events

ERCOFTAC Spring Festival
May 8^{th} 2014
Terrassa, Spain

ERCOFTAC Committee Meetings
May 9^{th} 2014
Terrassa, Spain

The ERCOFTAC Best Practice Guidelines for Industrial Computational Fluid Dynamics

The Best Practice Guidelines (BPG) were commissioned by ERCOFTAC following an extensive consultation with European industry which revealed an urgent demand for such a document. The first edition was completed in January 2000 and constitutes generic advice on how to carry out quality CFD calculations. The BPG therefore address mesh design; construction of numerical boundary conditions where problem data is uncertain; mesh and model sensitivity checks; distinction between numerical and turbulence model inadequacy; preliminary information regarding the limitations of turbulence models etc. The aim is to encourage a common best practice by virtue of which separate analyses of the same problem, using the same model physics, should produce consistent results. Input and advice was sought from a wide cross-section of CFD specialists, eminent academics, end-users and, (particularly important) the leading commercial code vendors established in Europe. Thus, the final document can be considered to represent the consensus view of the European CFD community.

Inevitably, the Guidelines cannot cover every aspect of CFD in detail. They are intended to offer roughly those 20% of the most important general rules of advice that cover roughly 80% of the problems likely to be encountered. As such, they constitute essential information for the novice user and provide a basis for quality management and regulation of safety submissions which rely on CFD. Experience has also shown that they can often provide useful advice for the more experienced user. The technical content is limited to single-phase, compressible and incompressible, steady and unsteady, turbulent and laminar flow with and without heat transfer. Versions which are customised to other aspects of CFD (the remaining 20% of problems) are planned for the future.

The seven principle chapters of the document address numerical, convergence and round-off errors; turbulence modelling; application uncertainties; user errors; code errors; validation and sensitivity tests for CFD models and finally examples of the BPG applied in practice. In the first six of these, each of the different sources of error and uncertainty are examined and discussed, including references to important books, articles and reviews. Following the discussion sections, short simple bullet-point statements of advice are listed which provide clear guidance and are easily understandable without elaborate mathematics. As an illustrative example, an extract dealing with the use of turbulent wall functions is given below:

- Check that the correct form of the wall function is being used to take into account the wall roughness. An equivalent roughness height and a modified multiplier in the law of the wall must be used.
- Check the upper limit on *y+*. In the case of moderate Reynolds number, where the boundary layer only extends to *y+* of 300 to 500, there is no chance of accurately resolving the boundary layer if the first integration point is placed at a location with the value of *y+* of 100.
- Check the lower limit of *y+*. In the commonly used applications of wall functions, the meshing should be arranged so that the values of *y+* at all the wall-adjacent integration points is only slightly above the recommended lower limit given by the code developers, typically between 20 and 30 (the form usually assumed for the wall functions is not valid much below these values). This procedure offers the best chances to resolve the turbulent portion of the boundary layer. It should be noted that this criterion is impossible to satisfy close to separation or reattachment zones unless *y+* is based upon *y**.
- Exercise care when calculating the flow using different schemes or different codes with wall functions on the same mesh. Cell centred schemes have their integration points at different locations in a mesh cell than cell vertex schemes. Thus the *y+* value associated with a wall-adjacent cell differs according to which scheme is being used on the mesh.
- Check the resolution of the boundary layer. If boundary layer effects are important, it is recommended that the resolution of the boundary layer is checked after the computation. This can be achieved by a plot of the ratio between the turbulent to the molecular viscosity, which is high inside the boundary layer. Adequate boundary layer resolution requires at least 8-10 points in the layer.

All such statements of advice are gathered together at the end of the document to provide a 'Best Practice Checklist'. The examples chapter provides detailed expositions of eight test cases each one calculated by a code vendor (viz FLUENT, AEA Technology, Computational Dynamics, NUMECA) or code developer (viz Electricité de France, CEA, British Energy) and each of which highlights one or more specific points of advice arising in the BPG. These test cases range from natural convection in a cavity through to flow in a low speed centrifugal compressor and in an internal combustion engine valve.

Copies of the Best Practice Guidelines can be acquired from:

ERCOFTAC CADO
Crown House
72 Hammersmith Road
London W14 8TH, United Kingdom

Tel: +44 207 559 1429
Fax: +44 207 559 1428
Email: magdalena.jakubczak@ercoftac.org

The price per copy (not including postage) is:

ERCOFTAC members	
First copy	*Free*
Subsequent copies	75 Euros
Students	75 Euros
Non-ERCOFTAC academics	140 Euros
Non-ERCOFTAC industrial	230 Euros
EU/non EU postage fee	10/17 Euros

Synthesis on the Activities of SIG36 "Swirling Flows" Concerning Rotation Effects

M. Braza[1] and P. Bontoux[2]

[1] *IMFT - UMR 5502 CNRS, Toulouse, France*
[2] *M2P2 - UMR 7340 CNRS, Marseille, France*

The present article regroups contributions of the following Institutes and Companies concerning swirling flows and rotation effects:

- The University of Liverpool
- The Laboratory M2P2, "Mécanique, Modélisation et Procédés Propres, UMR 7340 CNRS, - (Aix-Marseille Université) - Centrale Marseille France
- EXA Company GmbH
- The IMFT - Institut de Mécanique des Fluides de Toulouse, UMR 5502 CNRS-INPT-UPS, France
- The ICUBE, Laboratoire des Sciences de l'Ingé nieur, de l'Informatique et de l'Imagerie - UMR-7357
- Modelling & Simulation Centre, University of Manchester, STFC Daresbury Laboratory, Scientific Computing Department, Manchester, UK

These activities regrouped the investigation of the swirl effect and breakdown behind a wind turbine, the stability of Taylor-Couette flows with a radial temperature gradient, the oscillating rotor blades co-rotating disk pairs in turbomachinery and rotation effects around cylinders. The simulation methods used are direct numerical simulations, Lattice-Bolzmann methods, statistical LES and hybrid RANS-LES approaches. The major outcomes are presented in the following sections.

The stability of Taylor-Couette flow in respect of the radial temperature gradient has been investigated by detailed high-order DNS, under the effect of the main physical parameters governing the flow, the Taylor and Rayleigh numbers and involving the rotation rate of the inner cylinder in a quite tall, narrow-gap system. The thermal effects are taken into account by means of the Boussinesq approximation. Spiral roll instability regimes involving regular or wavy vortices have been quantified and analysed.

Furthermore, the rotation effects issued from the wall have been studied by DNS around a single cylinder, as well as for corotating disk pair configurations. Concerning the single cylinders, successive bifurcations and critical rotation rates have been evaluated by means of finite-element 3D Navier-Stokes methods. With regard to the corotating disks, DNS associating spectral methods have quantified the instabilities development in good agreement with experiments, with applications in storage of computing disks and turbomachinery. In these studies, the inner region between the disks has been found to be characterized by solid-body rotation. Turbulence effects are found to develop in the peripheral zone of the cavity and the development of a centrifugal instability governed by Rayleigh's criterion is analysed.

At higher Reynolds numbers, the wall rotation effects are analysed by means of the Lattice-Bolzmann numerical approach, allowing for use of very small time-steps and therefore removing time-discretisation uncertainties comparing to other methods, as well as the use of sliding grid approach, allowing as a perspective, a promising application to the whole rotor simulation. The studies carried out concern pitching flows around airfoils in respect of the dynamic stall, particularly interesting the helicopter blade industry, wind turbines and turbomachinery. The Lattice - Bolzmann approach has proven promising for the prediction of the drag and lift oscillating evolutions, comparing with results issued from URANS and hybrid RANS-LES methods studied in recent European research programs for the same high-Reynolds number configurations. In this context, adapted statistical approaches for capturing inhomogeneous turbulence effects have been used in URANS and in the statistical part of the Delayed Detached Eddy Simulation (as for example the Organised Eddy Simulation among other approaches), showing the ability of the method in capturing the hysteresis loops as well as their secondary oscillations due to the dynamic stall and the downstream of the trailing-edge vortex dynamics and pairing (including mushroom structures development). These approaches have been also successfully applied to wall rotation effects on a single cylinder in high Reynolds numbers. Furthermore, the Large Eddy Simulation provided quite promising results for the wall rotation around a circular cylinder at moderate Reynolds numbers, concerning the Flettner rotor problem.

In the high Reynolds number range, the efficiency of adapted URANS for the simulation of the whole swirl effect on wind turbine rotors has been investigated at high Reynolds number, by using the ALE formulation for the moving configuration and two-equation k-omega turbulence modelling. A successful capturing of the main dynamics (onset of instabilities with high frequency content and regular wake region with swirl effect) has been achieved over a long downstream distance, where the spiral swirl motion has been represented in quite good agreement with the physics.

The above aspects are presented in detail in the following sections.

The present overview has shown the ability of different simulation methods to capture complex phenomena induced by the swirling effect and the wall rotation in applications arising in aerodynamics, turbomachinery and energy (including wind turbines and Flettner-rotor type of propulsion due to rotation). A major part of the contributors are involved in symposia organized by ERCOFTAC and in European research programs of the FP7. By means of these collaborations, advancing in modelling and simulation methods is expected as well as continuation of collaborations in new European research programmes in the FP8, thanks to scientific and technical interactions favorised by ERCOFTAC. The SIG36 plans to organise an international workshop in autumn 2015 in France with the contribution of the AU"M, Association Française de Mécanique" and the GDR "Groupement De Recherche" - 2865 - Turbulence of CNRS, among other Institutions, where the state-of-the-art in swirling flows and wall-rotation effects will be presented.

Breakdown of the Swirling Wake Behind a Wind Turbine

M. Carrión, M. Woodgate, R. Steijl and G.N. Barakos

CFD Laboratory, School of Engineering, University of Liverpool, Liverpool, L63 3GH, U.K.

Abstract

This work explores the breakdown of the wake downstream a wind turbine rotor and assesses the capability of CFD in predicting its correct physical mechanism. The wake is resolved on a fine mesh able to capture the vortices up to 8 rotor radii downstream of the blades. In the stable wake region, the wake fell on a perfect spiral and the main harmonic present in the flow was the blade passing frequency. In the region of the onset of instabilities, higher frequency content was present, and resulted in vortex pairing.

1 Introduction

Accurate predictions of wind turbine wakes are important for the performance analysis of the turbines and their optimal positioning within tightly-spaced wind farms. In the past, CFD was considered a tool confined to the near-wake analysis due to the inherent numerical dissipation of CFD solvers. With progress, however, in numerical methods and mesh density, CFD is emerging as a good tool for the analysis of the wakes since it can accurately capture the development of core instabilities that will lead to the wake breakdown. Ivanell et al. [1] studied the stability of tip vortices in an azimuthally periodic domain using the actuator-line method (one blade was simulated with spatial periodicity assumed). Perturbations were added to the solution and it was found that when the oscillations of vortices from one spiral to the next were out of phase the instabilities were larger than for in-phase modes. Likewise, the non-linear development of the wake instability resulted in vortex pairing.

Attemps to predict the wind turbine wake breakdown with CFD methods are present in the literature. However, in some works an azimuthally periodic domain was employed [1], restricting therefore the azimuthal wave number of the instabilities to be multiple of the number of blades. Likewise, in many publications instead of employing the full blade representation, the actuator line or actuator disk techniques were used [2, 3, 4]. With the latter, no individual vortices can be captured and both blade models require very detailed tabulated data, which makes the wake breakdown study very difficult. It was also found that most works lack the grid resolution required for wake study [5, 6]. This, along with the numerical dissipation, tends to trigger artificial wake decay. For a detailed wake study, the grid needs to be sufficiently fine to capture individual vortices with several cells accross their diameter, and it should be nearly uniform without any sudden changes, to have minimal numerical dissipation.

2 Numerical Method

The Helicopter Multi-Block (HMB2) code [7] of Liverpool is used for the present work, and has so far been validated using the NREL Annex XX experiments [8] and MEXICO project [9]. HMB2 solves the Navier-Stokes equations in integral form using the arbitrary Lagrangian Eulerian (ALE) formulation for time-dependent domains with moving boundaries:

$$\frac{d}{dt}\int_{V(t)} \vec{\mathbf{w}}dV + \int_{\partial V(t)} \left(\vec{F}_i\left(\vec{\mathbf{w}}\right) - \vec{F}_v\left(\vec{\mathbf{w}}\right)\right)\vec{n}dS = \vec{S} \quad (1)$$

where $V(t)$ is the time dependent control volume, $\partial V(t)$ its boundary, $\vec{\mathbf{w}}$ is the vector of conserved variables $[\rho, \rho u, \rho v, \rho w, \rho E]^T$. $\vec{F_i}$ and $\vec{F_v}$ are the inviscid and viscous fluxes, including the effects of the mesh movement. For steady-state rotor simulations, the grid is not rotating. A source term $\vec{S} = [0, -\rho\vec{\omega} \times \vec{u}_h, 0]^T$ is instead added to compensate for the inertial effects of the rotation along with a velocity assigned to grid nodes. $\vec{u}_h$ is the local velocity field in the rotor-fixed frame of reference. The Navier-Stokes equation are discretised using a cell-centred finite volume approach on a multi-block grid, leading to the following equations:

$$\frac{\partial}{\partial t}\left(\mathbf{w}_{i,j,k}V_{i,j,k}\right) = -\mathbf{R}_{i,j,k}\left(\mathbf{w}_{i,j,k}\right) \quad (2)$$

where $\mathbf{w}$ represents the cell variables and $\mathbf{R}$ the residuals. i, j and k are the cell indices and $V_{i,j,k}$ is the cell volume. Osher's [10] upwind scheme is used to discretise the convective terms and MUSCL [11] variable interpolation is used for nominally third order accuracy. The Van Albada limiter [12] is used to reduce the oscillations near steep gradients. Temporal integration is performed using an implicit dual-time step method. The linearised system is solved using the generalised conjugate gradient method with a block incomplete lower-upper (BILU) pre-conditioner [13]. To account for low-speed flows, the Low-Mach Roe scheme (LM-Roe) [14] is used instead of the Osher's scheme.

Multi-block structured meshes are generated using the ICEM-Hexa$^{\mathrm{TM}}$of ANSYS. For rotor flows, a typical multi-block topology used in the University of Liverpool is described in [15].

For the present study, RANS computations were performed, since they do not march in real time and therefore results can be obtained faster than with time-accurate simulations. Likewise, the k-ω turbulence model by Wilcox [16] was employed, due to its stability and the presence of attached flow on the blades for the studied wind speeds.

3 Simulations Setup

In the present work, a chimera grid [17] was employed, which permits localised grid refinement. In the computations assuming periodicity in space (single-blade domain), an 860 million cells mesh was employed, which consists of 3 chimera levels, as shown in 1. Firstly, a coarse background that extends from 4R upstream to 12R downstream the rotor and a blade-fitted grid with a C-topolgy for optimally resolving the boundary layer. The mesh region for the wake capture extends from the blade's root up to 1.6R in the radial direction and 8R behind the rotor plane. In this region, the cells have a size of 2.5% of the chord at the blade's root (6mm) in the axial and radial directions, covering 0.22 degrees in the azimuthal direction. With this resolution, 24 cells capture the vortex core.

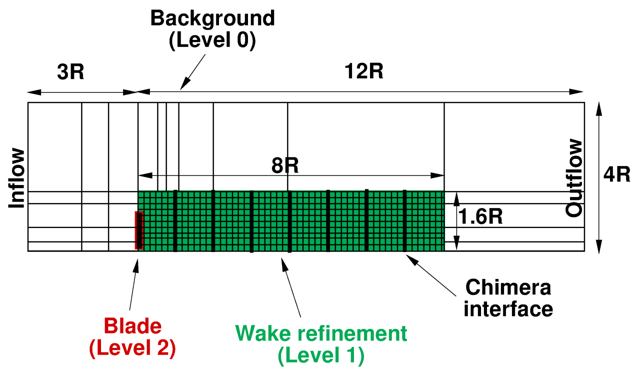

Figure 1: Computational domain, including dimensions in radii and three chimera levels

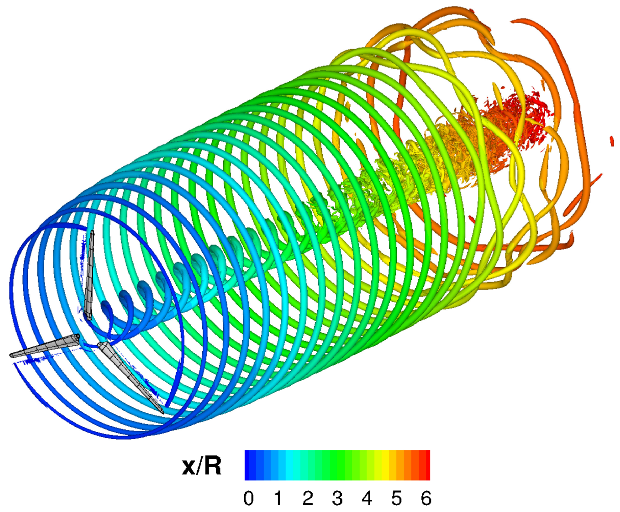

(a) Wake at 15m/s.

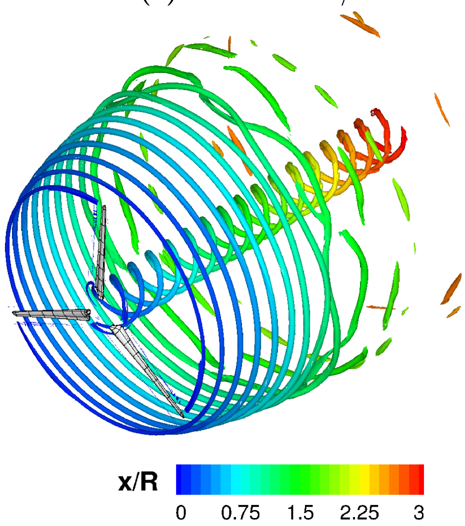

(b) Wake at 10m/s.

Figure 2: Wake developed behind the MEXICO rotor visualised with iso-surfaces of $\lambda_2 = -0.01$

4 Results and Discussion

4.1 Vortex evolution

Iso-surfaces of λ_2-criterion [18] are employed to visualise the swirling wake behind the wind turbine. At 15m/s wind speed, 2 (a), the wake falls on a perfect spiral until 4R, approximately, and between 4-5R (sixth revolution) the vortex core has an oscillatory behaviour, which indicates the presence of instabilities. For 10m/s, 2 (b), there is more expansion in the wake and the oscillatory behaviour is observed from 1.25R, corresponding to the third rotor revolution. Since in both cases the rotor rotates at a constant rate of 424.5rpm, the wake takes 0.7 and 0.28 seconds to be unstable, respectively.

The vorticity contours presented in 3 (a) show that at 15m/s the vortices are equidistant until 4R downstream, where the tip vortices begin to pair. From that point, there is a strong vortex interaction. It is also interesting that the vortices are perfectly round until 2R downstream and, from that point, become elliptical until the pairing begins. For the lower wind speed case shown in 3 (b), the vortex pairing starts at 1.25R. This is due to the fact that in this case the vortices are closer to each other and, therefore, the mutually induced velocity strain is higher. It is also noteworthy that the root vortices seem to be stable further downstream than the tip vortices. This should be attributed to the higher blade pitch at the root which, in absence of hub, leads to longer distances between vortices, making therefore the self-induced flow between them lower. Additionally, a discontinuity in the wake can be observed at approximately 70% R span-wise position. At that blade station, two different aerofoils (RISO-A1-21 and NACA-64-418) are blended and this discontinuity might be due to differences of their zero-lift angles. At 50% R, there is also a change in aerofoil sections (DU91-W2-250 and RISO-A1-21), but the effect seems to be smaller.

4 shows planes parallel to the rotor at two axial locations. Firstly, 4 (a) shows the region where the vortices describe a perfect spiral, denoted as *stable wake*. The *unstable wake* is shown in 4 (b), where the instabilities are developed, and the tip vortices start to interact between them describing an oscillatory pattern as suposed to a perfect circle.

4.2 Vortex core size

A comparison between the measured vortex in the experiments and the computed with CFD is presented in 5, for a 120-degree old vortex (t=0.047s), where good agreement is observed. The shear spiral generated as the vortex spins, which can be observed in light colour surrounding the measured vortex core (5 (a) and (c)), is well captured in the CFD (5 (b) and (d)).

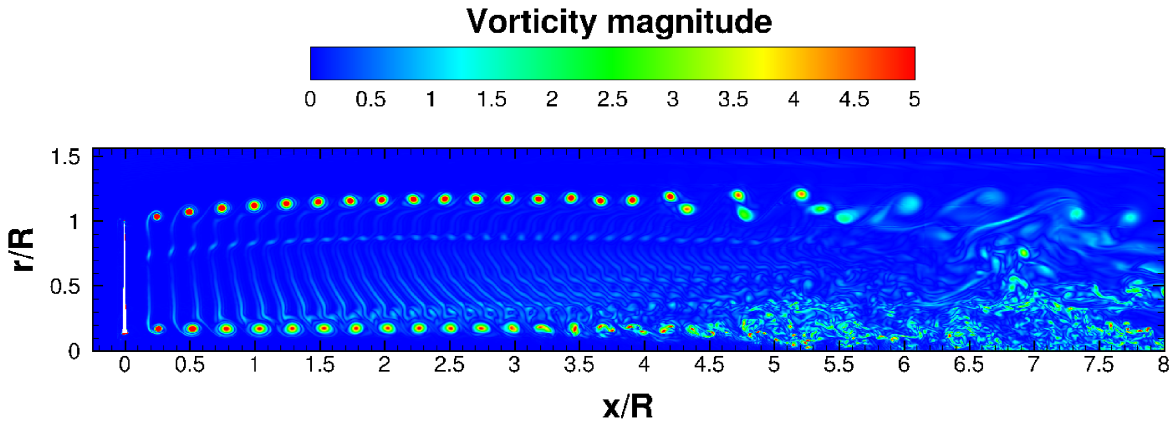

(a) Wake at 15m/s wind speed ($\lambda = 15$).

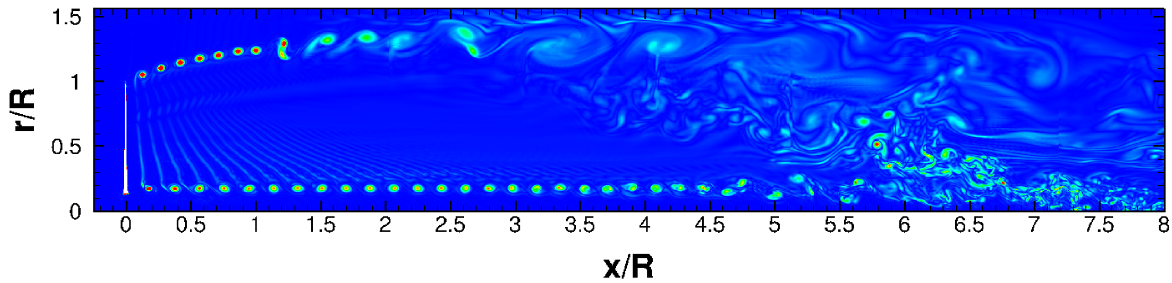

(b) Wake at 10m/s wind speed ($\lambda = 10$).

Figure 3: Vorticity contours in planes perpendicular to the rotor through a blade at 12 o'clock

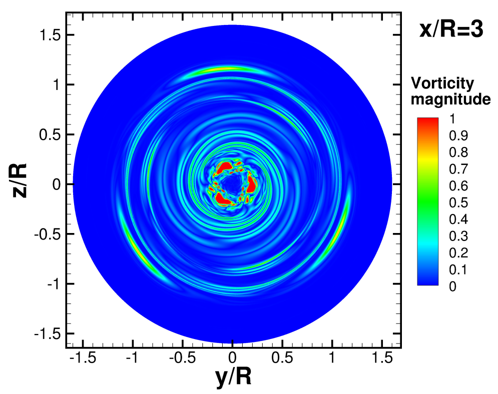

(a) $x/R = 3$.

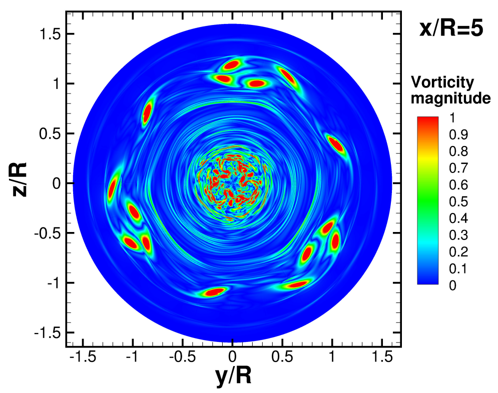

(b) $x/R = 5$.

Figure 4: Planes parallel to the rotor plane at two axial locations, for 15m/s wind speed

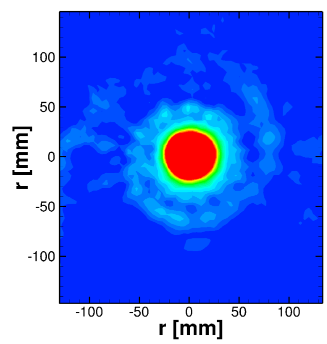

(a) 15m/s (EXP).

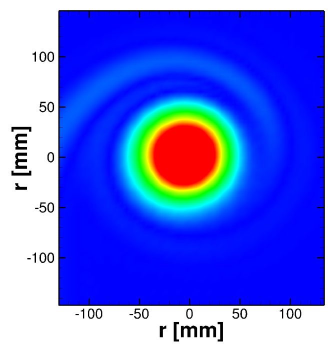

(b) 15m/s (CFD).

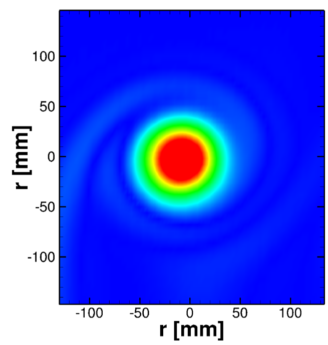

(c) 10m/s (EXP).

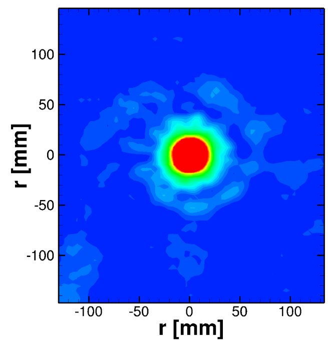

(d) 10m/s (CFD).

Figure 5: Comparison between the experimental (EXP) and computed (CFD) 120-dgree old vortex

The tangential velocity ratio (v/v_{peak}) across the 120-degree old vortex is shown in 6. For a better comparison, and since there are uncertainties concerning the experiments and the blade tip shape, the radial coordinate has been normalised with the experimental vortex radius ($r_{c_{10}}$ =14mm and $r_{c_{15}}$ =22mm) and the CFD vortex radius ($r_{c_{10}}$ =37.5mm and $r_{c_{15}}$ =42mm), respectively for both cases. To quantify how diffusive the vortices are, the Vatistas empirical model [19] is employed, where the non-dimensional tangential velocity can be written as,

$$v = \frac{\overline{r}}{(1+\overline{r}^{2n})^{1/n}}, \tag{3}$$

where $\overline{r} = r/r_c$ and n is a positive integer parameter. The lower the value of n, the more diffusive is the vortex and when $n = \infty$ the perfect Rankine profile is obtained. As can be seen in both wind speed cases, the CFD solution follows the trend of the Vatistas model between $n = 2$ and $n = 3$, showing small diffusion.

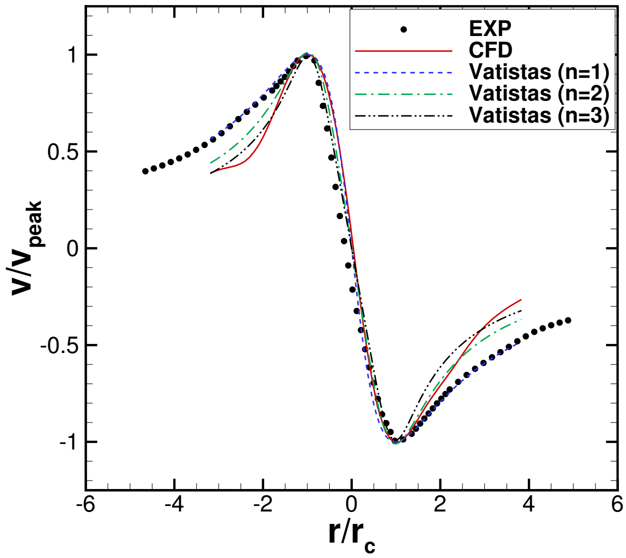

(a) 10m/s.

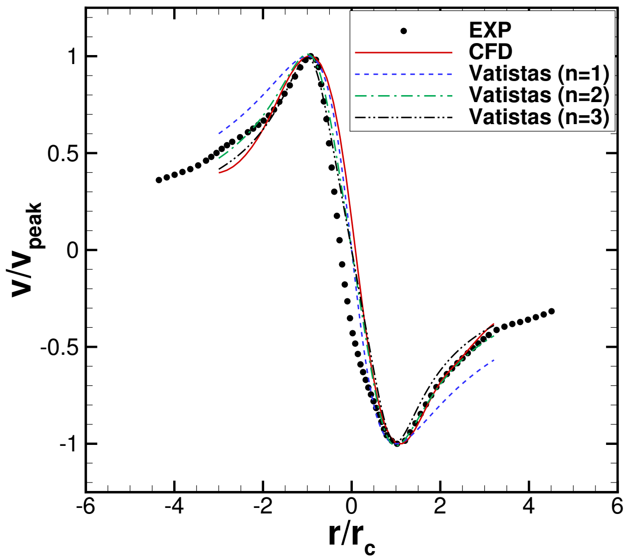

(b) 15m/s.

Figure 6: Radial velocity ratio across the vortex for the 120-degrees old vortex. Comparison with experiments [9] and Vatistas model [19]

4.3 Growth of instabilities

A series of sampling data covering different axial positions where extracted in the wake, to obtain the velocity signals and their correspondant FFT. The set of probes were located in a radial station coinciding with the tip of the blade and from the rotor plane to 6R in the streamwise direction. Since the CFD was steady-state, the space domain can be converted into time domain, using $t = \frac{\Psi}{\omega}$; where Ψ is the azimuthal position and ω the rotational frequency. 3600 samples of velocity data were extracted, which is equivalent to 1.41s signal (10 rotor revolutions).

Since the rotational frequency is 7.075Hz and the rotor has 3 blades, the first harmonic is 21.2Hz, which corresponds to the blade-passing frequency. The results show a frequency of 21.4Hz, and second and third harmonics of 42.8Hz and 64.2Hz, respectively. For the unstable wake region, frequencies up to 300Hz were also captured. This is the result of the interaction between vortical structures that leads to their breakdown into smaller ones. Taking as a reference that each blade covers 7 revolutions every second (7Hz), these high frequency structures cover 1/42 times that distance or, in other words, a 1/6 of a circumference. This can be easily visualised in the tip vortices of 4 (b).

The amplitudes of the u velocity component at 15m/s wind speed from the rotor plane to 6R downstream for these three first harmonics are shown in 7. From 1R to 3R approximately, the amplitudes are almost constant and the main frequency content is the rotational one (21.4Hz). Likewise, from 3R to 4.5R an approximate exponential growth can be observed, until it reaches a value of Δu = 1.4m/s. From that point, the second and third harmonics become important, leading to the oscillatory behaviour and vortex pairing discussed in Section 4.1. This is in good agreement with an earlier study presented by Ivanell et al.[1], where the amplitudes of a prescribed perturbation where tracked in the streamwise direction. In the initial wake evolution, the same exponential growth was obtained and the multiples of the first harmonic were dominant in the vortex pairing region.

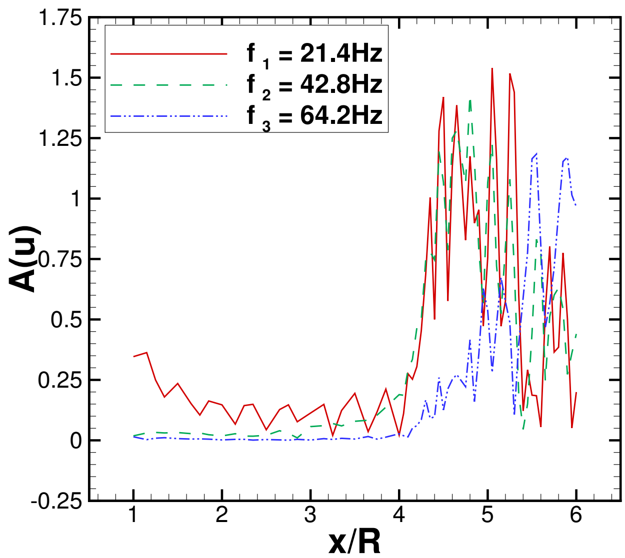

Figure 7: Amplitudes of axial velocity for the first three harmonics, as a function of the axial position, for the 15m/s wind speed case

5 Conclusions

The swirling wake developed behind the MEXICO rotor was identified and instabilites leading to vortex pairing from 4R downstream for wind speed of 15m/s were observed, as a result of the vortex interaction. At 10m/s wind speed, the vortices were closer to each other leading to higher self-induced flow and stronger interaction, which resulted in instabilities at 1.25R, approximately. The computed vortices were well preserved downstream and, in the stable wake region, they showed good agreement with the experiments. FFTs of the axial velocity component enabled to identify the main harmonics in the wake. For the stable wake, the main frequency was the blade-passing one and where instabilites were present higher frequencies dominated.

The results suggest that CFD methods are able to predict instabilities on wind turbine wakes.

Acknowledgements

The computations were performed on the N8 HPC facility "Polaris" at Leeds University, and the Hartree HPC Centre of U.K. Access to both systems is gratefully acknowledged, as well as the financial support by the National Renewable Energy Center of Spain (CENER) and the University of Liverpool. The use of the MEXICO experimental data is also acknowledged.

References

[1] S. Ivanell, R. Mikkelsen, J. Sorensen, and D. Henningson, "Stability analysis of the tip vortices of a wind turbine," *Wind Energy*, vol. 13, pp. 705–715, 2010.

[2] N. Troldborg, J. Sorensen, and R. Mikkelsen, "Numerical simulations of wake characteristics of a wind turbine in uniform flow," *Wind Energy*, vol. 13, pp. 86–99, 2010.

[3] N. Troldborg, F. Zahle, P.-E. Rethore, and N. Sorensen, "Comparison of the wake of different types of wind turbine CFD models," in *5th AIAA Aerospace Sciences Meeting including the New Horizons Forum and Aerospace Exposition*, Nashville, Tennessee, January 2012.

[4] C. Gundling, H. Gopalan, B. Roget, and J. Sitamaran, "A free-vortex wake diffusion model for wind turbines in steady and turbulent atmospheric inflow," in *51st AIAA Aerospace Science Meeting*, Grapevine (Dallas/Ft. Worth Region), Texas, January 2013.

[5] J.-O. Mo, A. Choudhry, and M. A. Y.-H. Lee, "Large eddy simulation of the wind turbine wake characteristics in the numerical wind tunnel model," *J. Wind Eng. Ind. Aerodyn.*, vol. 112, pp. 11–24, 2013.

[6] J.-O. Mo, A. Choudhry, M. Arjomandi, R. Kelso, and Y.-H. Lee, "Effects of wind speed changes on wake instability of a wind turbine in a virtual wind tunnel using large eddy simulation," *J. Wind Eng. Ind. Aerodyn.*, vol. 117, pp. 38–56, 2013.

[7] G. Barakos, R. Steijl, K. Badcock, and A. Brocklehurst, "Development of CFD capability for full helicopter engineering analysis," in *31st European Rotorcraft Forum*, Florence, Italy, September 2005.

[8] M.M. Hand and D.A. Simms and L.J. Fingersh and D.W. Jager and J.R. Cotrell and S. Schreck and S.M. Larwood, "Unsteady aerodynamics experiment phase VI: wind tunnel test configurations and available data campaigns," *Technical report TP-500-29955, NREL*, 2001.

[9] J.G. Schepers and H. Snel, "Final report of IEA Task 29, MexNext (Phase I): Analysis of Mexico wind tunnel measurements," *Technical report, ECN*, 2012.

[10] S. Osher and S. Chakravarthy, "Upwind Schemes and Boundary Conditions with Applications to Euler Equations in General Geometries," *Journal of Computational Physics*, vol. 50, pp. 447–481, 1983.

[11] B. van Leer, "Towards the Ultimate Conservative Difference Scheme, V. A Second Order Sequel to Godunov's Method," *J. Comp. Phys.*, vol. 32, pp. 101–136, 1979.

[12] G. van Albada, B. van Leer, and W. Roberts, "A Comparative Study of Computational Methods in Cosmic Gas Dynamics," *Astron. Astrophysics*, vol. 108, pp. 76–84, 1982.

[13] O. Axelsson, *Iterative Solution Methods*. Cambridge University Press: Cambridge, MA, 1994.

[14] M. Carrión, M. Woodgate, R. Steijl, and G. Barakos, "Implementation of All-Mach Roe-type Schemes in Fully Implicit CFD Solvers - Demonstration for Wind Turbine Flows," *International Journal for Numerical Methods in Fluids*, vol. 73, pp. 693–728, 2013.

[15] R. Steijl and G. Barakos and K. Badcock, "A framework for CFD analysis of helicopter rotors in hover and forward flight," *International Journal for Numerical Methods in Fluids*, vol. 51, pp. 819–847, 2006.

[16] D. Wilcox, "Multiscale Model for Turbulent Flows," *AIAA Journal*, vol. 26, pp. 1311–1320, 1988.

[17] M. Jarkowski and M. Woodgate and G. Barakos and J. Rokicki, "Towards Consistent Hybrid Overset Mesh Methods for Rotorcraft CFD," *International Journal for Numerical Methods in Fluids*, vol. 74, pp. 543–576, 2014.

[18] J. Jeong and F. Hussain, "On the Identification of a Vortex," *Journal of Fluid Mechanics*, vol. 285, pp. 69–94, 1995.

[19] G. Vatistas, V. Kozel, and W. Mih, "A Simpler model for concentrated vortices," *Experiments in Fluids*, vol. 11, pp. 73–76, 1991.

Indeterminate Regime in an Enclosed Corotating Disk Pair

A. Randriamampianina

Laboratoire M2P2 UMR 7340, CNRS, Aix-Marseille Université, École Centrale Marseille
randria@l3m.univ-mrs.fr

Research Activities

Indeterminate regime in an enclosed corotating disk pair

The Enclosed Corotating Disk Pair (ECDP) configuration is formed by two corotating disks delimited by an inner cylinder, the hub, corotating with the disks and an outer, stationary casing. Applications include mainly computer disk storage systems and disk cavities in turbomachinery.

Direct numerical simulations based on high resolution spectral methods are carried out to investigate the indeterminate regime observed experimentally by [1] for small values of gap ratio. The flow is characterized by the presence of a turbulent zone towards the periphery of the cavity, where the strong velocity gradient generated at the junction of the rotating disks and the stationary shroud is unstable according to Rayleigh's criterion for centrifugal instability. The flow may be divided into five distinct regions : the inner region near the hub in solid-body rotation (which satisfies the Taylor-Proudman theorem), the outer region dominated by vortical structures, the separation zone between these two regions, the Stewartson boundary layer along the fixed shroud and the Ekman layers along the two disks.

In the present case, the geometry is defined by a gap ratio $G \equiv s/(b-a) = 0.2$ and a radius ratio $a/b = 0.5$, where a and b are the inner and outer radius and s is the distance between the two disks. The rotation rate corresponds to a rotational Reynolds number $Re \equiv \Omega b^2/\nu = 2 \times 10^4$. In a previous work [2], it was found that below a critical gap ratio limit $G < G_c = 0.258$, the transition from axisymmetric to three-dimensional solutions occurs via time-dependent behaviours, unlike the pitchfork bifurcation for larger values of the gap ratio $G > G_c$. The solution was found to remain axisymmetric and steady up to $Re = 1.575 \times 10^4$, before becoming unsteady. Moreover, unlike the solutions obtained for values of gap ratio $G > G_c$ in [2] , where the first three-dimensional flow was laminar, the flow enters directly a spatio-temporal chaotic behaviour.

The separation zone between the inner and outer regions has a polygonal shape as illustrated in 1(a) in agreement with the visualization reported in [1]. It constitutes a detached shear layer resulting from the meeting of the three-dimensional vortical structures in the outer region with the two-dimensional flow in the inner region governed by solid-body rotation. This layer is found to act like a compliant surface and its shape moves with the vortices in the outer region, which precess relative to the disks.

The turbulence activity is observed in the outer region characterized by successive pairing of vortices aligned in the axial direction rotation and parallel to the azimuthal direction, as shown in 1(b) and as mentioned by [1]. A Rankine (combined free and forced) vortex structure was identified for the flow, as already observed in [2]. The outer region is composed of two separate zones in the meridional (r, z) plane, which exhibit symmetry breaking with respect to the inter-disk midplane. This structure results from the centripetal jetlike flow arising from the outer casing and fed by the radial outward Ekman layers developing along the two disks. The detached shear layer acting like a compliant surface, this flapping flow remains restricted in the outer region. The locations of this centripetal jet along the shroud show a wavy structure as illustrated in 1(c). These locations fluctuate randomly over time, which may explain the vibrational modes observed in computer disk storage systems.

This work was granted access to the HPC resources NEC-SX5 of IDRIS (CNRS, France) under the allocation 20744 made by GENCI "(Grand Equipement National de Calcul Intensif)".

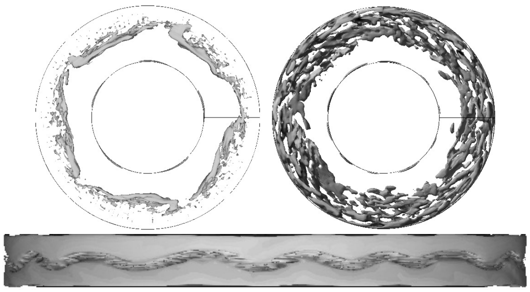

Figure 1: Instantaneous flow characteristics : (a) detached shear layer in the (r, θ) plane; (b) vortical structures in the outer region in the (r, θ) plane; (c) flapping centripetal jet locations at the shroud in a (r, z) plane

References

[1] S. D. Abrahamson, J. K. Eaton, and D. J. Koga, "The flow between corotating disks," *Phys. Fluids*, vol. A 1(2), pp. 241–251, 1989.

[2] A. Randriamampianina, R. Schiestel, and M. Wilson, "Spatio-temporal behaviour in an enclosed corotating disk pair," *J. Fluid Mech.*, vol. 434, pp. 39–64, 2001.

Lattice-Boltzmann Simulations of an Oscillating NACA0012 Airfoil in Dynamic Stall

A.F.P. Ribeiro, D. Casalino and E. Fares

Exa GmbH, Curiestrasse 4, 70563, Stuttgart, Germany
andre@exa.com

1 Introduction

Dynamic stall occurs when airfoils change their angle of attack quickly, delaying flow separation when the angle is increasing, and producing a maximum lift coefficient (C_L) which is higher than that of static cases. During pitch down, C_L is generally lower than the static counterparts, since the flow requires time to reattach to the upper surface of the airfoil. This phenomenon is particularly relevant to flapping wings and to the helicopter industry, since helicopter blades vary rapidly in pitch during forward flight.

The use of Computational Fluid Dynamics (CFD) for oscillating airfoils has been increasing over the past few years. Most simulations are done with Unsteady Reynolds-Averaged Navier-Stokes (URANS) simulations [1, 2, 3], usually for relatively low angles of attack, since this method has several shortcomings when it comes to massively separated flows. Martinat et al. [4] accomplished URANS and Detached Eddy Simulations (DES) on a low Reynolds number airfoil, but DES did not show much improvement over URANS. To the authors' knowledge, Large Eddy Simulation (LES) has been applied to low Reynolds number cases only [5]. The state of the art of using high-fidelity simulations for oscillating airfoils can be observed in the DESider CFD validation project [6], which chose as a basic test case for dynamic stall the flow around a NACA0012 airfoil at Reynolds number $Re = 0.98 \cdot 10^6$, Mach number $M = 0.072$, reduced pitching frequency $k_f = 0.1$ ($k_f = \omega c/(2U_\infty)$, where ω is the oscillation frequency, c is the chord, and U_∞ is the freestream velocity), and angle of attack varying between 5deg and 25deg. DESider results showed DES compared more favorably with experiments than URANS, although discrepancies were observed for both methods.

The experiments by McCroskey [7] used in many CFD validation studies (including DESider) have shown to be challenging to match with numerical simulations. For C_L the main difficulties are in the prediction of the trends at the maximum and minimum values, around 22deg and 10deg, for pitch up and down, respectively. For the drag coefficient (C_D) the sudden rise on pitch up around 21deg and smooth drop on pitch down around 20deg are the main issues. The moment coefficient (C_M) results vary by a large margin and even capturing the overall trend has been demonstrated to be very difficult, even using computationally more demanding DES. To the authorsâĂŹ knowledge, no LES were performed for this case so far.

Among the several open questions regarding the uncertainties affecting the experimental data, those related to the wind tunnel walls will be demonstrated to play a major role in the discrepancy between measurements and predictions. Since none of the DESider participants used moving meshes, these effects could not be estimated and far-field simulations were performed instead. Another uncertainty was related to laminar to turbulent transition. Since the experimental data did not have unsteady transition measurements, fully turbulent simulations were performed. A consistent parametric study on the spanwise length of the airfoil and the effect of the boundary conditions on the side walls is also lacking. On the numerical uncertainty, there were concerns in the DESider project [6] regarding the physical time step length. From a pragmatic point of view, it is also necessary to include moving meshes in this case for it to be applicable to industrially relevant cases.

The present paper revisits the McCroskey et al. [7] test case used in DESider in an attempt to contribute to the aforementioned open questions. A parametric study on the wind tunnel effects is conducted, where the size of the tunnel and the use of free-slip and no-slip boundary conditions are tested, i.e. taking into account wind tunnel blockage and boundary layer growth effects. An efficient explicit solver is used, and hence a very small time step is also introduced. Furthermore, a detailed look at the flow field is presented, in order to better understand the dynamic stall phenomenon. The Lattice-Boltzmann Method (LBM) with Very Large Eddy Simulations (VLES) is used as an alternative to classic Navier-Stokes simulations. A sliding mesh is employed to rotate the airfoil within the wind tunnel test section. This method has been recently used to reproduce hysteresis for a high-lift wing in slow pitching movement [8].

2 Numerical method

Simulations were carried out using the Lattice-Boltzmann [9, 10] software PowerFLOW 5.0a, in 3 dimensions and 19 velocity states, with the collision term modeled with the well-known BGK approximation [11], and the equilibrium distribution approximated by a third order expansion [12] with constant temperature [13]. Fluid quantities such as density and momentum can be retrieved from LBM using the Chapman-Enskog expansion [14], which can then lead to the compressible Navier-Stokes equations [15, 16]. However, in contrast to the Navier-Stokes equations, the current method is based on linear formulation which relies on simple computational operations, allowing for efficient, accurate, and highly scalable implementations, with an explicit time advancement scheme.

For high Reynolds flows, turbulence modeling is introduced [17] by solving a variant of the RNG $k-\varepsilon$ model [18] on the unresolved scales [19], selected via

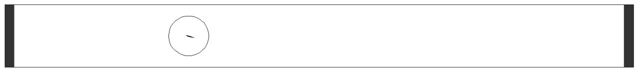

Figure 1: Simulation domain and sliding mesh outline

a swirl model [20], a method referred to as LBM Very Large Eddy Simulation (LBM-VLES). An extended wall model including pressure gradient effects is used in the near-wall region [21].

The LBM scheme is solved on a grid composed of cubic volumetric elements (voxels). A variable resolution by a factor of two is allowed between adjacent regions. Consistently, the time step is varied by a factor two between two adjacent resolution regions. Solid surfaces are automatically facetized within each voxel intersecting the wall geometry using planar surface elements, surfels [9].

Time advancement is performed with an explicit scheme, which allows for efficient, highly scalable simulations. For the present simulations, the number of time steps per full angle of attack cycle is around 700000.

The sliding mesh approach uses two reference frames, one body-fixed and one ground-fixed (or wind tunnel-fixed). Two-sided surfels are used between the body-fixed and the ground-fixed meshes and mass, momentum, and heat fluxes are exactly conserved across the interface [22].

The numerical methods described have been extensively validated for a wide variety of applications ranging from academic cases using DNS [23] to industrial flow problems in the fields of aerodynamics [24, 25], thermal management [24], and aeroacoustics [26, 27]. The sliding mesh approach was recently employed in the aforementioned slow pitching of a high-lift wing [8].

3 Simulation setup

The case setup was done trying to match the experiment as close as possible. The wind tunnel geometry is included, with a height of about $5c$ and a spanwise length of about $3.5c$. The domain is shown in 1. It extends $20c$ upwind and $50c$ downwind, where the velocity inlet and pressure outlet were positioned, respectively. The main reason to include the wind tunnel walls is that the results by McCroskey et al. [7] differ significantly from the results by McAlister et al. [28], which were obtained in the same wind tunnel, but with an airfoil twice as large. Some information on the exact geometry of the wind tunnel is not available in the literature (e.g. the boundary layer thickness on the wind tunnel walls and the exact geometry of the small gaps between the airfoil and the walls), hence the present conditions do not match the experiments exactly. However, they should be sufficient to test the sensitivity of the flow field to the wind tunnel and predict the overall trends in the following parametric studies.

The Cartesian grid is prepared automatically by PowerFLOW based on boxes and offsets defined *a priori*. A sliding mesh with arbitrary, time dependent angular velocity is employed in a cylinder of $2.3c$ spanning the whole domain and centered at $0.25c$.

Experimental data [7] is available for C_D, C_L, and C_M as functions of the angle of attack. The data was phase-averaged over 50 cycles, since the results varied from one cycle to the next. The aerodynamic coefficients were obtained in experiment by integrating surface pressure in the middle section of the airfoil with a trapezoidal rule. The simulations presented here were run for five cycles, with the first two cycles being discarded from the comparison. In preliminary simulations it was seen that running longer did not affect the trends of the aerodynamic coefficients noticeably. Forces are integrated over the whole airfoil surface and include friction as well as pressure.

4 Results

The results of the LBM simulations are presented in this section. A grid convergence study was performed on 2D static simulations, in order to choose the grid used for the dynamic simulations. Then, 2D dynamic simulations were performed to investigate the effects of the height of the wind tunnel test section. Increasing the wind tunnel size by a factor of 4 caused significant changes to the aerodynamic coefficients, indicating that the inclusion of the wind tunnel walls is important to match the experimental results. These 2D simulations are not reported here for the sake of brevity. The 3D dynamic simulations are presented and compared to 2D and experimental results in the following sections.

4.1 3D dynamic simulations

Two 3D simulations were performed: a case with free-slip boundary conditions on all wind tunnel walls, labeled 3D Free-Slip WT; and a similar case, but with no-slip wind tunnel walls, labeled 3D No-Slip WT. The spanwise length of both cases is $3.5c$ and matches the one used in the wind tunnel. The objective of the latter simulation is to investigate the near wall separation effects on the overall aerodynamic behavior of the oscillating airfoil.

2 shows a comparison between the 2D Free-Slip WT case and 3D Free-Slip WT. Even though the results are different, there is only a small qualitative improvement using the 3D simualtions during the pitch down phase. During pitch up the 2D and 3D results are quite similar, since the flow is attached. The current 3D simulations do not have deterministic values during pitch down, with all cycles being slightly different from the others, while 2D results consistently alternated between two polars.

The two 3D simulations, with Free-Slip and No-Slip wind tunnel are presented in 3. The peak values are better predicted with no-slip boundary conditions and all coefficients have their magnitude reduced during pitch down, approaching the experiments. Drag and moment stall occur sooner and less abruptly. The reason for that will be shown in section 4.2. The large oscillations of lift during pitch down are reduced with no-slip side walls, due to the vortices being less coherent, as will be discussed in section 4.2.

4 shows the values of C_M for both 3D cases. The free-slip case is significantly over predicting the magnitude of CM during pitch down, which does not happen for the no-slip case. The differences during pitch up are more noticeable for C_M than for C_L and C_D, with two peaks near the maximum value and a difference of the maximum value of more than 20%. The large sensitivity of C_M to the wind tunnel walls could explain why it was the quantity with most disagreement with experiments for the DESider participants [6].

4.2 Flow analysis

In order to understand the behavior of the flow displayed in the plots of the previous section, an analysis of the unsteady flow structures was performed. 5 shows instantaneous static pressure on the surface of the airfoil,

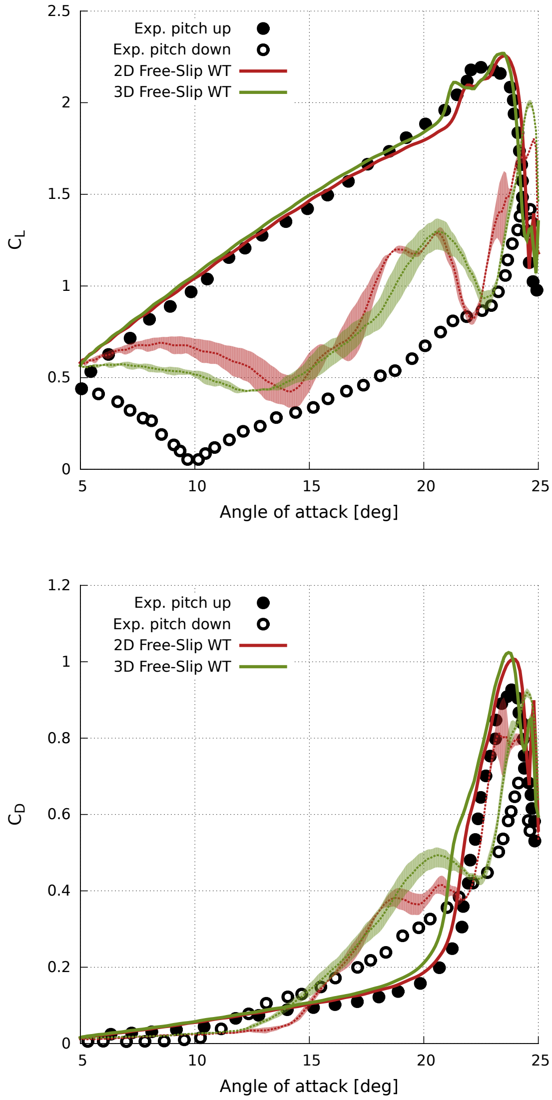

Figure 2: Lift (C_L) and drag (C_D) coefficients for both free-slip wind tunnel cases

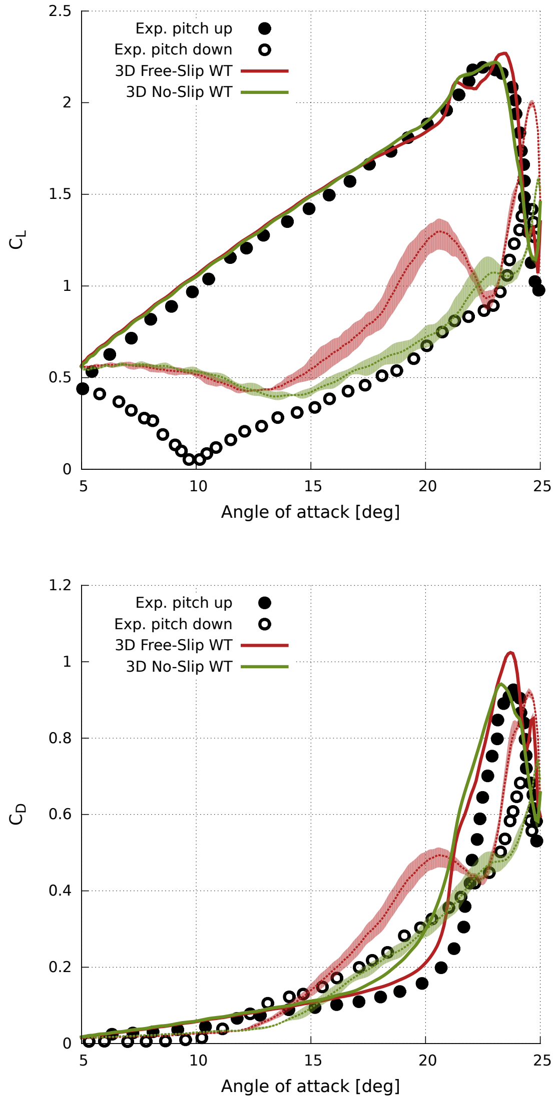

Figure 3: Lift (CL) and drag (CD) coefficients for both 3D cases

iso-surfaces of λ_2 [29] in half of the simulation domain in spanwise direction, colored by velocity magnitude (non-dimensionalised by the freestream velocity) in grayscale, and streamlines on a slice close to the side wall for three different angles of attack of both 3D cases. On pitch up the two cases start to become different around 18deg, where corner separations appear on the no-slip case. By the time the leading edge vortex is formed, around 22deg, the corner vortices are very developed, while the free-slip case has no separation other than the aforementioned vortex. After that, both cases exhibit very separated flow, but the trailing edge vortices are much stronger and more coherent in the free-slip case.

The strong suction near the trailing edge of the free-slip case explains the high peaks of C_M seen in the previous section, which were also present in the DESider simulations. The difference between the two cases presented here show how sensitive the flow is to the side walls boundary condition. Hence, simulating this flow with periodic or symmetry boundary conditions seems unreasonable and it is not surprising that matching the experimental values has been difficult in previous numerical studies. The current results are still not in perfect agreement with the measurements during pitch down,

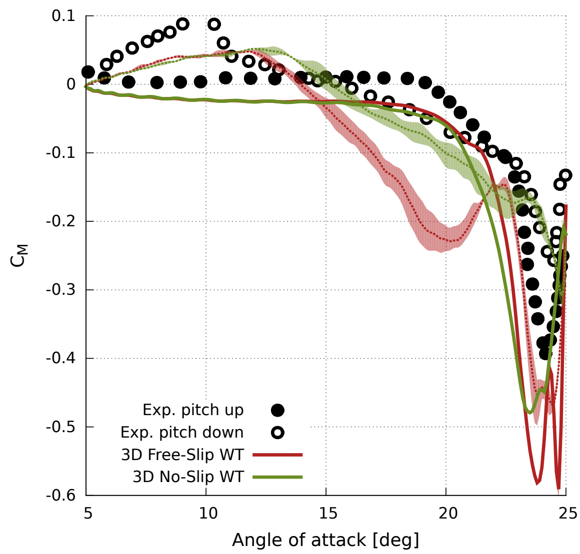

Figure 4: Moment coefficient (C_M) for both 3D cases

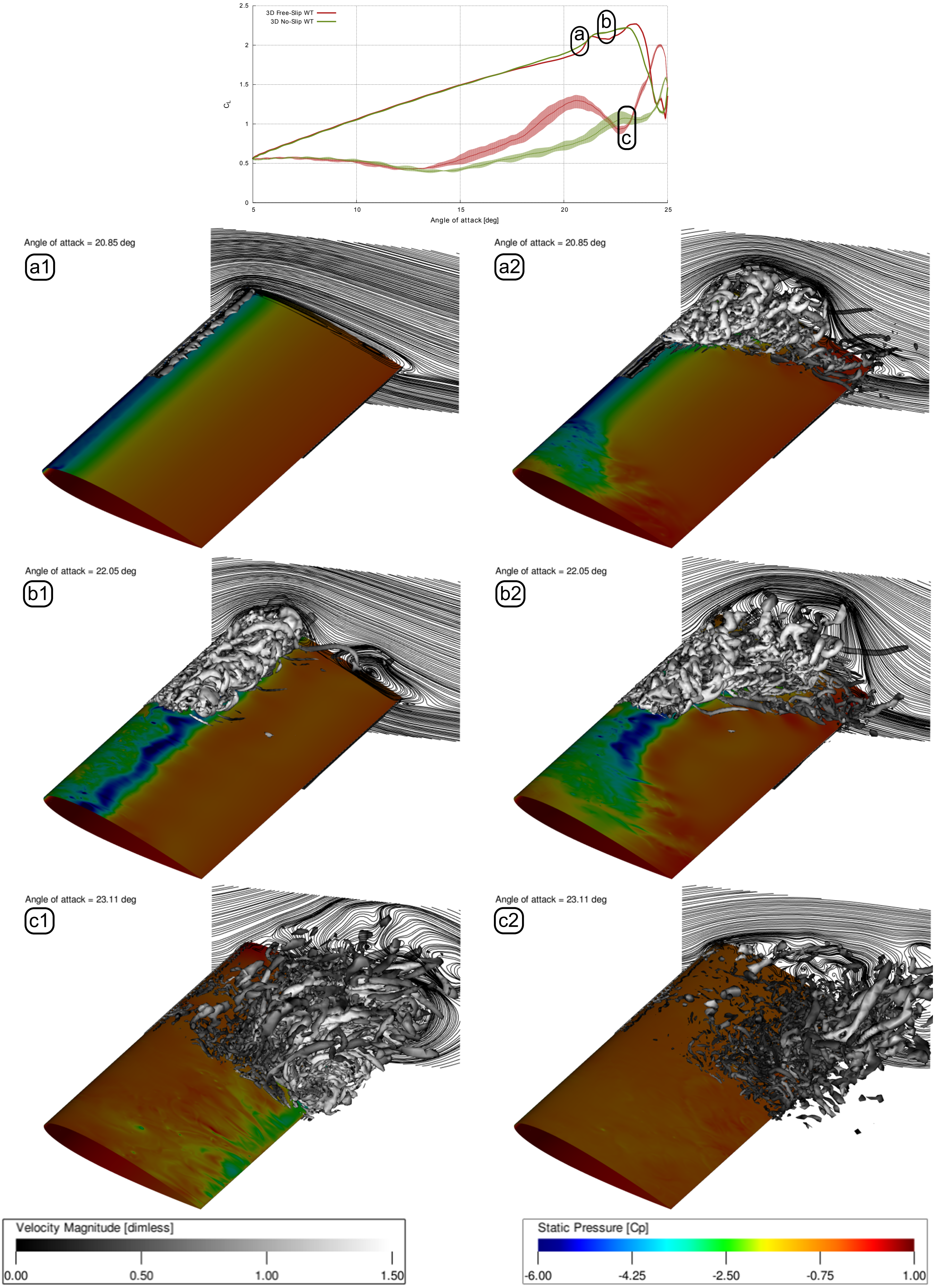

Figure 5: Lift coefficient (C_L) polar at the top. Instantaneous static pressure on the surface of the airfoil, iso-surfaces of λ_2 in half of the domain, colored by velocity magnitude in grayscale, and streamlines on a slice for both 3D cases. Letters correspond to different points on the lift curve. Number 1 and 2 correspond to 3D Free-Slip WT and 3D No-Slip WT, respectively

but the authors believe that this is due to the fact that the wind tunnel is still not represented precisely, without the right boundary layer thickness and geometric gaps between the airfoil model and side mountings present in the experiments.

The earlier separation seen in 5 a2 explains the earlier drag stall that occurs for the no-slip case in 3. This would not be captured by the experiments, since the pressure was measured in the center line and then integrated to obtain the aerodynamic coefficients. To measure the impact of such procedure, the drag polar is shown again in 6 for the 3D No-Slip WT case, but obtained in two different ways: the first results, are obtained by integrating the forces along the entire airfoil surface; the second results integrate the forces on a slice of $0.5c$ in the centerline, neglecting the effects near the side walls. Clearly the drag stall angle is closer to experiments when measured in the center line.

Lift stall also approaches the experimental values by integrating the forces on the center line only. 7 shows C_M for the same cases of 6, where the moment stall is also sharper for the center line case, consistent with the drag stall. The fluctuations decrease for the full surface integration case because the forces are averaged over a larger area, smoothing out the local peaks along the span.

5 Conclusions

The LBM solver PowerFLOW 5.0a was employed for 2D and 3D simulations of an oscillating NACA 0012. The sensitivity to the wind tunnel presence was studied in 2D, where the lift slope and stall angles varied with the size of the wind tunnel. This could explain the reason for discrepancies in previously published simulations by other authors.

Including the side walls of the wind tunnel in the 3D simulations was shown to have a large impact on the results, particularly during pitch down. Measuring the forces in the center section, as in the wind tunnel, improved even more the agreement with experiments. This also explains some of the disagreement observed in previous studies. To the authorsâĂŹ knowledge, no similar simulations were done before.

Results compare favorably with experiments for C_D and for most of the C_L curve. The reasons for the disagreement in C_M are still unclear, although the experiments are expected to have uncertainties for this quantity larger than 0.05 for $M < 0.1$, especially in stalled regions [7]. Qualitative and quantitative improvements of aerodynamic coefficients in comparison to recent DESider DES results [6] were achieved, which is expected to be associated with the wind tunnel side walls effects taken into account in the present work. A very small time step was employed, so the uncertainties in time discretization are minimal. The introduction of the sliding mesh is an important step towards applying this methodology to full helicopter simulations.

Future work could focus on matching the experimental conditions even more, by reproducing the boundary layer thickness on the wind tunnel wall and including the small gaps between the airfoil and the side walls. The low Reynolds number of the experiments also indicates that transition modeling could play a role in the aerodynamics. New experiments with fewer uncertainties regarding the conditions and measurements would be major contributions to the study of dynamic stall and for further numerical validation.

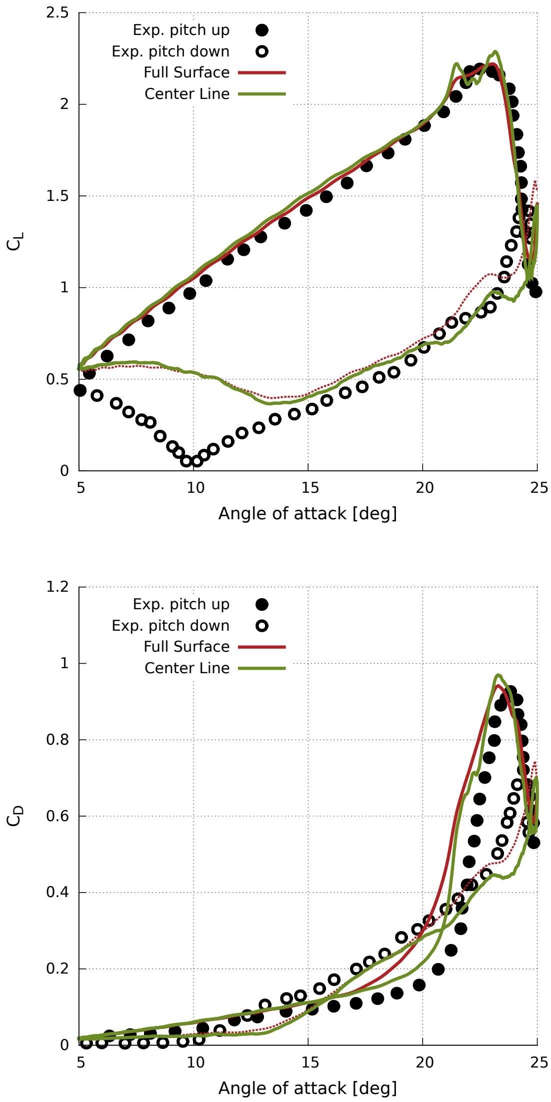

Figure 6: Lift (C_L) and drag (C_D) coefficients for 3D No-Slip WT case integrating forces on the full airfoil surface and on the center line only

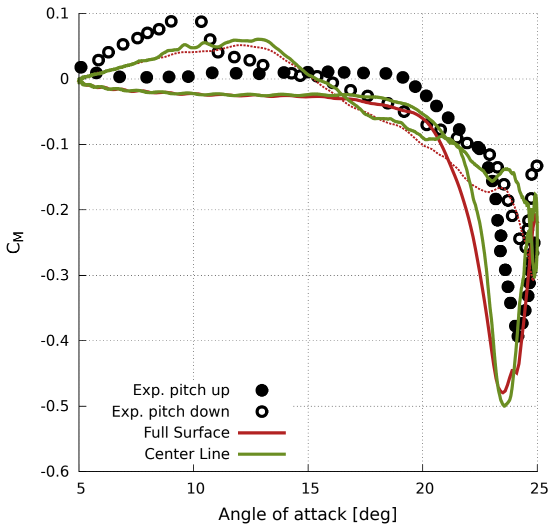

Figure 7: Moment coefficient (CM) for 3D No-Slip WT case integrating forces on the full airfoil surface and on the center line only

Acknowledgements

The authors are grateful to Dr. Alistair Revell for providing the experimental data, and to Dr. Ignacio Gonzalez for the help in formatting this paper.

References

[1] J. Ekaterinaris and F. Menter, "Computation of Oscillating Airfoil Flows with One- and Two-Equation Turbulence Models," *AIAA Journal*, vol. 32, pp. 2359–2365, 1994.

[2] A. Spentzos, *CFD Analysis of 3D Dynamic Stall.* Phd thesis, University of Glasgow, 2005.

[3] C. Marongiu, *On the Aerodynamic Force of the Oscillating Airfoils.* Phd thesis, UniversitÃă degli Studi di Napoli Federico II, 2009.

[4] G. Martinat, M. Braza, Y. Hoarau, and G. Harran, "Turbulence modelling of the flow past a pitching NACA0012 airfoil at 105 and 106 Reynolds numbers," *Journal of Fluids and Structures*, vol. 24, pp. 1294–1303, 2008.

[5] S. Nagarajan, S. Hahn, and S. Lele, "Prediction of Sound Generated by a Pitching Airfoil: A Comparison of RANS and LES," in *AIAA Paper 2006-2516*, 2006.

[6] W. Haase, M. Braza, and A. Revell, "DESider - A European Effort on Hybrid RANS-LES Modelling," in *Notes on Numerical Fluid Mechanics and Multidisciplinary Design 103*, 2009.

[7] W. McCroskey, K. McAlister, L. Carr, and S. Pucci, "An experimental study of dynamic stall on advanced airfoil sections volume 1. summary of the experiment," Tech. Rep. NASA TM 84245.

[8] E. Fabiano, E. Fares, , and S. N olting, "Unsteady Flow Simulation of High-Lift stall Hysteresis using a Lattice Boltzmann Approach," in *AIAA Paper 2012-2922*, 2012.

[9] H. Chen, C. Teixeira, and K. Molvig, "Realization of Fluid Boundary Conditions via Discrete Boltzmann Dynamics," *International Journal of Modern Physics C*, vol. 9, no. 8, pp. 1281–1292, 1998.

[10] S. Chen and G. Doolen, "Lattice Boltzmann Method for Fluid Flows," *Annual Review of Fluid Mechanics*, vol. 30, pp. 329–364, 1998.

[11] P. Bhatnagar, E. Gross, and M. Krook, "A Model for Collision Processes in Gases. I. Small Amplitude Processes in Charged and Neutral One-Component Systems," *Physical Review*, vol. 94, no. 3, pp. 511–525, 1954.

[12] H. Fan, R. Zhang, and H. Chen, "Extended volumetric scheme for lattice Boltzmann models," *Physical Review E*, vol. 73, no. 066708, 2006.

[13] H. Chen and C. Teixeira, "H-theorem and origins of instability in thermal lattice Boltzmann models," *Computer Physics Communications*, vol. 129, pp. 21–31, 2000.

[14] S. Chapman and T. Cowling, *The Mathematical Theory of Non-Uniform Gases.* London: Cambridge University Press, 1990.

[15] H. Chen, S. Chen, and W. Matthaeus, "Recovery of the Navier-Stokes Equations Using a Lattice-Gas Boltzmann Method," *Physical Review A*, vol. 45, pp. 5339–5342, 1992.

[16] X. Shan, X.-F. Yuan, and H. Chen, "Kinetic theory representation of hydrodynamics: a way beyond the Navier-Stokes equation," *Journal of Fluids Mechanics*, vol. 550, pp. 413–441, 2006.

[17] H. Chen, S. Kandasamy, S. Orszag, R. Shock, S. Succi, and V. Yakhot, "Extended boltzmann kinetic equation for turbulent flows,"

[18] V. Yakhot, S. A. Orszag, S. Thangam, T. B. Gatski, and C. G. Speziale, "Development of turbulence models for shear flows by a double expansion technique," *Physics of Fluids A*, vol. 4, no. 7, pp. 1510–1520, 1992.

[19] C. M. Teixeira, "Incorporating turbulence models into the Lattice-Boltzmann Method," *International Journal of Modern Physics C*, vol. 9, pp. 1159–1175, 1998.

[20] C. Alexander, H. Chen, S. Kandasamy, R. Shock, and S. Govindappa, "Simulations of Engineering Thermal Turbulent Flows Using a Lattice Boltzmann Based Algorithm," in *ASME PVP*, 2001.

[21] A. Anagnost, A. Alajbegovic, H. Chen, D. Hill, C. Teixeira, and K. Molvig, "Digital Physics Analysis of the Morel Body in Ground Proximity," in *SAE Paper 970139*, 1997.

[22] R. Zhang et al., "Lattice Boltzmann approach for local reference frames," vol. 9, 2011.

[23] Y. Li, R. Shock, R. Zhang, and H. Chen, "Numerical Study of Flow Past an Impulsively Started Cylinder by Lattice Boltzmann Method," *Journal of Fluid Mechanics*, vol. 519, pp. 273–300, 2004.

[24] E. Fares, S. Jelic, T. Kuthada, and D. Schroeck, "Lattice Boltzmann Thermal Flow Simulation and Measurements of a modified SAE Model with Heated Plug," in *Proceedings of FEDSM2006, FEDSM2006-98467*, 2006.

[25] G. Bres, D. Williams, and T. Colonius, "Numerical Simulations of Natural and Actuated Flow over a 3D, Low-Aspect-Ratio Airfoil," in *AIAA Paper 2010-4713*, 2010.

[26] R. Satti, R. Shock, and S. Noelting, "Aeroacoustic Analysis of a High Lift Trapezoidal Wing using lattice Boltzmann Method," in *AIAA Paper 2008-3048*, 2008.

[27] A. Ribeiro, D. Casalino, E. Fares, and S. Noelting, "CFD/CAA Analysis of the LAGOON Landing Gear Configuration," in *AIAA Paper 2013-2256*, 2013.

[28] M. K.W., L. Carr, and W. McCroskey, "Dynamic stall experiments on the naca 0012 airfoil," Tech. Rep. NASA TP 1100.

[29] J. Jeong and F. Hussain, "On the identication of a vortex," *Journal of Fluid Mechanics*, vol. 285, pp. 69–94, 1995.

Stability of Taylor-Couette Flows With a Radial Temperature Gradient

S. Viazzo and S. Poncet

Aix-Marseille Université, CNRS, École Centrale Marseille, Laboratoire M2P2 UMR 7340

The influence of a radial temperature gradient on the stability of Couette-Taylor flow has been investigated by extensive direct numerical simulations. The cavity is characterized by a narrow gap $\eta = R_i/R_o = 0.8$ and a high aspect ratio $\Gamma = H/(R_o - R_i) = 80$ (R_i and R_o the radii of the inner and outer cylinders and H their height) corresponding to the experimental set-up developed by Guillerm [1]. The flow depends mainly on two physical parameters: the Taylor number $Ta = \Omega R_i d(d/R_i)^{1/2}/\nu$ and the Rayleigh number $Ra = g\alpha\Delta T d^3/(\nu\kappa)$, with $d = R_o - R_i$ and Ω the rotation rate of the inner cylinder. 28 cases have been computed for $Ta = [11 - 150]$ and $Ra = [1166 - 13228]$ to enable direct comparisons with the experiments of Guillerm [1].

The numerical method is based on the 2D compact fourth-order projection decomposition method of Abide and Viazzo [2], extended to cylindrical coordinates on non-staggered grids. The time advancement is second-order accurate. The derivatives are approximated using fourth-order compact formula in the radial and axial directions and Fourier series in the azimuthal direction. Due to the large aspect ratio, the domain is axially decomposed into 8 subdomains using the influence matrix technique. The thermal effects are considered using the Boussinesq approximation. Each sub-domain contains $K = 64$ Fourier modes over 2π and $N \times M = 61 \times 61$ grid points in the radial and axial directions respectively. The time step δt varies in the range $[2 - 4]$ ms.

The aim is to characterize all the flow patterns occuring in the system for various Rayleigh and Taylor numbers. Under isothermal conditions ($Ra = 0$), the Taylor Vortex Flow regime (TVF) is first recovered at a critical Taylor number equal to $Ta = 48$ and above a second threshold $Ta = 56$, DNS results report the classical Wavy Vortex Flow regime (WVF, 1f). In the non-isothermal case, the stability diagram shows a large variety of instability patterns appearing as spirals, wavy vortices or the coexistence of both shown in 1 in terms of temperature maps. The Partial SPIral regime (PSPI) observed by Guillerm [1] appears as regular helicoidal vortices located at the bottom of the cavity. The PSPI regime has not been obtained here confirming the numerical study of Kedia et *al*. [3], who reported a direct transition from the axisymmetric TVF to a regular spiral flow for $Ta = 50$ ($\eta = 0.5$ and 0.7) around $Ra \simeq 910$. It is probably due to experimental imperfections in the thermal heating not included in the numerics. Moreover, it has been carefully checked that the flow and thermal fields are similar to the base state even in the vicinity of the endcap disks, which supposes also a direct transition to the regular spiral regime (SPI, 1b). The six other instability regimes have been recovered by DNS for different combinations of (Ra, Ta). The temperature maps in 1 clearly show that endcap effects are relatively weak and confined in the vicinity of the disks. At low Rayleigh numbers, for example $Ra = 2063$, the first transition leads to the appearance of the SPIral regime. Even for

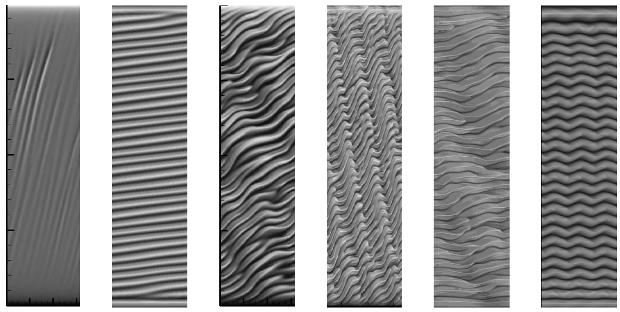

(a) (b) (c) (d) (e) (f)

Figure 1: Temperature maps obtained by DNS in a $(\theta = [0, 2\pi], z = [0, h])$ plane at mid-radius highlighting 6 different instabilities: (a) MSPI ($Ra = 7150$, $Ta = 11$), (b) SPI ($Ra = 1166$, $Ta = 50$), (c) SPI+D ($Ra = 7150$, $Ta = 40$), (d) WSPI ($Ra = 7150$, $Ta = 75$), (e) SPI+WVF ($Ra = 7150$, $Ta = 90$), (f) WVF ($Ra = 7150$, $Ta = 150$)

a slight departure from the critical Taylor number, the spirals invade the whole system. These helicoidal vortices are very regular along the axial direction with only weak endwall effects close to the top and bottom stationary disks. Above a second threshold, these spirals may coexist with a Wavy Vortex Flow, regime denoted SPI+WVF (1e). Increasing further the Taylor number leads to a progressive encroachment of the wavy vortices in the whole system. Finally, above a third threshold, the WVF regime is obtained because of the progressive decreasing influence of the thermal effects compared to the inertial ones. At larger Rayleigh numbers, for example $Ra = 13228$, the base flow destabilizes at $Ta = 11.3$ in agreement with Guillerm [1] with the appearance of the Modulated SPIral regime (MSPI, 1a). These modulated spirals are characterized by the alternation of spirals with laminar flow regions. They are matched by groups and are observed in the whole cavity but for a very narrow range of Taylor numbers. Above a second threshold, the flow switches to the regime denoted SPI+D, for SPIrals with Dislocations (1c). This pattern is very irregular as the spirals are affected by numerous defects and dislocations. Thus, their inclination angle strongly varies depending on their spatial location. Increasing further the Taylor number induces the third instability regime: the Wavy SPIral regime (WSPI, 1d). The spirals get wavy with a temporal and spatial variation of their inclination angle. The two following regimes are successively the SPI+WVF and the WVF regimes already evoked for low Rayleigh numbers.

The heat transfers have been also discussed in terms of the averaged Nusselt numbers calculated along both walls as: $Nu = \frac{-\Delta R}{\Delta T}\frac{\partial T}{\partial r}|_w$. 2 clearly shows that the Nusselt numbers along the rotor increases for increasing values of the Taylor number. The averaged Nusselt

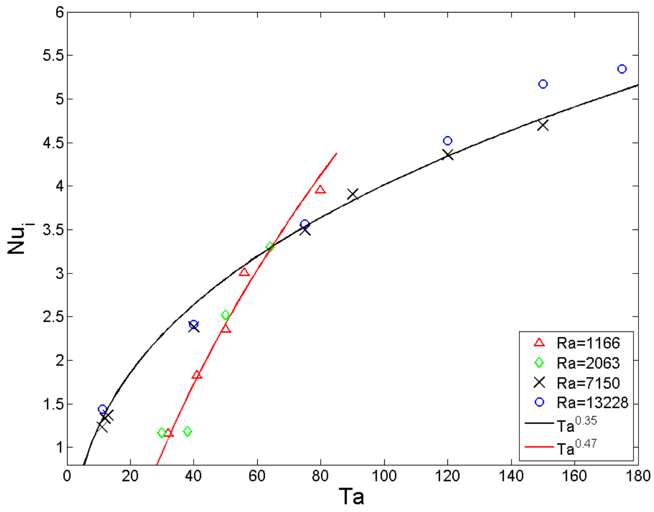

Figure 2: Distributions of the averaged Nusselt number against the Taylor number Ta along the rotor (Nu_i)

number along the stator Nu_o (not shown here, [4]) is besides slightly lower than Nu_i along the rotating wall: $Nu_o \simeq 0.78 Nu_i \simeq \eta Nu_i$. For all values of the Rayleigh number Ra, Nu remains close to unity at very low Taylor numbers $Ta < 40$ on both sides. At larger Ta values, two different behaviors are observed in the present simulations. For large Rayleigh numbers $Ra \geq 7150$, the DNS results are well fitted by $Nu \propto Ta^n$ with $n = 0.35$ and 0.3 on the inner and outer cylinders respectively and the Rayleigh number has only a weak effect on the Nusselt distribution. It perfectly falls between the values predicted by the boundary layer theory: $n = 1/2$ in the laminar regime and $n = 2/7$ in the turbulent regime. For $Ra \leq 2063$, a similar behavior is observed with $n = 0.47$ and 0.45 along the rotor and stator respectively.

As a conclusion, one reports the first high-order DNS of Taylor-Couette flows subjected to a radial temperature gradient in a very tall narrow-gap system. Seven over the eight instability regimes appearing as spiral rolls (MSPI, SPI, SPI+D, WSPI), regular (TVF) or wavy vortices (WVF) or a combination of both (SPI+WVF) observed experimentally by Guillerm [1] have been recovered by DNS. The only discrepancy concerns the partial spiral regime not observed here and which may be attributed either to heating asymmetries in the experiments or to the experimental procedure. Further calculations are then required to clarify this point and to go into more details on the secondary instability mechanisms. For more details about the main characteristics of the spirals close to the threshold of the primary instability and the variations of the moment coefficient and the averaged Nusselt numbers, the reader can refer to Ref.[4] or contact: *viazzo (at) l3m (dot) univ-mrs (dot) fr.*

References

[1] R. Guillerm, *Etude expérimentale des instabilités thermo-hydrodynamiques dans un système de Couette-Taylor.* PhD thesis, Université du Havre, 2010.

[2] S. Abide and S. Viazzo, "A 2D compact fourth-order projection decomposition method," *J. Comp. Phys.*, vol. 206, pp. 252–276, 2005.

[3] R. Kedia, M. Hunt, and T. Colonius, "Numerical simulations of heat transfer in Taylor-Couette flow," *J. Heat Transfer*, vol. 120, pp. 65–71, 1998.

[4] S. Viazzo and S. Poncet, "Stability of a high aspect ratio Taylor-Couette flow submitted to a radial temperature gradient," *under revision, Computers & Fluids*, 2014.

Wall Rotation Effects Around Bodies at Low And High Reynolds Numbers

G. Martinat[1], El Akoury[1], Y. Hoarau[2], D. Ruiz[3], G. Harran[1] and M. Braza[1]

[1] *Institut de Mécanique des Fluides de Toulouse, IMFT- UMR CNRS 5502, France*
[2] *ICUBE, Université de Strasbourg, UMR CNRS 7357, France*
[3] *IRIT, Institut de Recherche en Informatique, UMR 5505 CNRS - INPT - UPS, France*

IMFT - Institut de Mécanique des Fluides de Toulouse - UMR 5502 CNRS-INPT-UPS in collaboration with ICUBE and IRIT Institutes

1 Introduction

The research team "Interaction Fluide-Structure sous Turbulence" of the Institut de Mécanique des Fluides de Toulouse, UMR CNRS - INPT - UPS No 5502 in collaboration with the institute ICUBE at Strasbourg carried out a detailed physical analysis concerning wall rotation effects around bluff bodies and rotor blades by DNS (low Reynolds number) and by advanced URANS and Hybrid (RANS-LES) turbulence modelling.

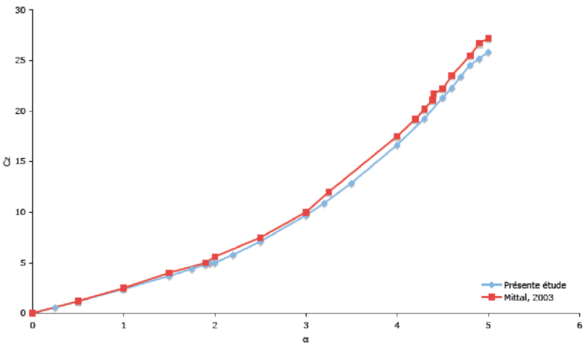

Figure 1: Evolution of the lift coefficient verus the rotation rate around a circular cylinder, DNS at Re=200

The successive bifurcations undergone by a rotating cylinder flow as the rotation rate increases has been studied in detail by means of the "in-house" numerical code ICARE in finite-element version, developed in collaboration with IRIT (Institut de Recherche en Informatique de Toulouse), research group APO and involving the researchers D. Ruiz, P. Amestoy and M. Dayde (director of IRIT) in the context of the PhD thesis of G. Martinat. By means of DNS, the evolution of the lift coefficient versus the rotation rate has been studied (figure 1, Martinat) in comparison with other studies (Mittal, 2004).

The evolution of the Strouhal number concerning the vortex shedding mode versus the rotation rate, presented in figure 2 shows the disappearance of the vortex shedding within the interval of (2, 4.3) and beyond the rotation rate of 5. In these intervals, the flow becomes steady, as shown in figure 3. When the flow develops vortex shedding, the vortex street is asymmetric due to the global shear imposed by the rotation, as shown in figure 4.

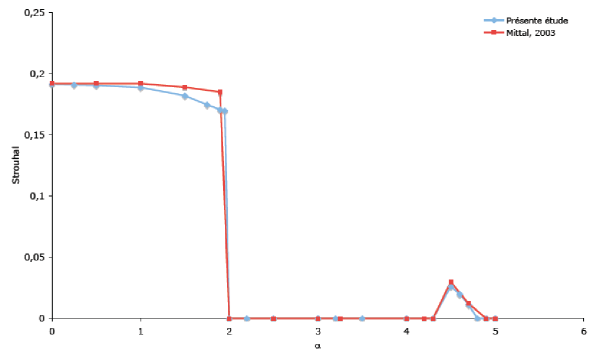

Figure 2: Evolution of the Strouhal number versus the rotation rate, DNS

By using adapted turbulence modelling closures in URANS and in Hybrid (RANS-LES) methods, the coherent structure dynamics are suitably solved by modelling the incoherent, random turbulence in the context of the OES, Organised Eddy Simulation (Braza, Perrin, Hoarau, (2006), Bourguet, Braza, El Akoury, Harran, (2008), Moussaed et al (2013)), figure 5. OES reinforces the near-wall turbulence-stress anisotropy by means of a tensorial eddy-viscosity concept, derived from the Differential Reynolds Stress transport modelling (DRSM), Haase, Braza, Revell (2009). Furthermore, it provides modified turbulence length and time scales by means of stochastic forcing of the turbulence kinetic energy and dissipation equations (Hunt et al (2013)), that improve the prediction of the thin shear-layer interfaces, a crucial issue for aeroacoustics and for capturing the wall rotation effects which generate highly shearing interfaces. The modified turbulence scales by means of OES are also used in the context of hybrid RANS-LES modelling approaches, in particular in the framework of DDES, Delayed Detached Eddy Simulation, yielding the DDES-OES modelling (figures 5 and 14).

Figures 6 to 9 present the grid and results for a wind turbine at Reynolds number 25000 (Martinat, 2007). The gain obtained by the turbine versus time is presented in figure 7. A zoom of the coherent structures around the turbine blades is presented on figure 9. Figures 10 to 13 present numerical simulations of oscillating wings in pitching motion at high Reynolds number in comparison with experiments carried out by Berton et al (2003).

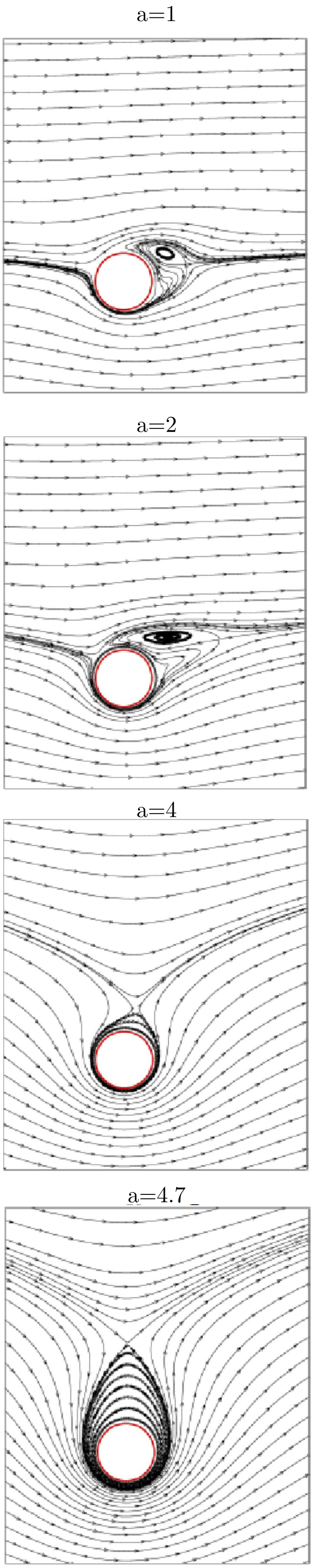

Figure 3: Modification of the flow structure as a function of the rotation rate

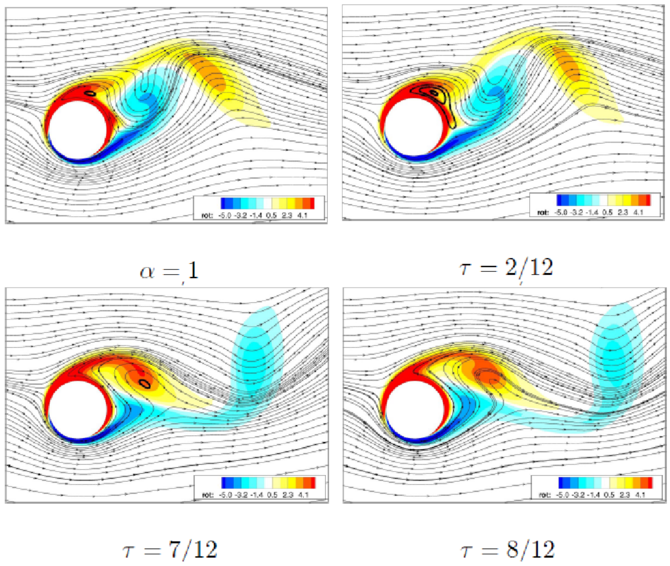

Figure 4: Vortex shedding evolution for the rotation rate alpha=1. DNS at Reynolds number 200

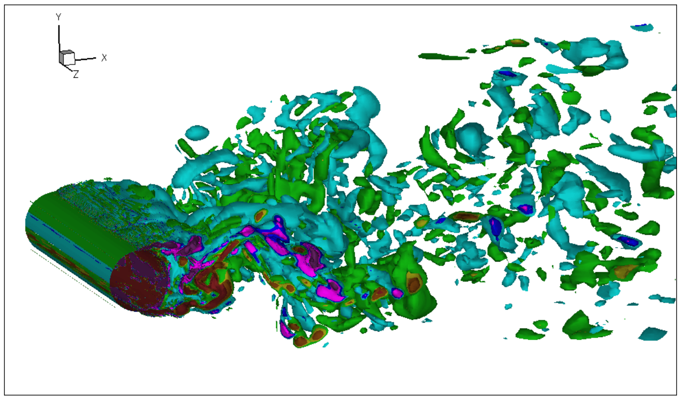

Figure 5: Coherent and incoherent near-wall structure capturing by the DDES-OES modelling, Moussaed et al, ERCOFTAC Symposium, June 2013)

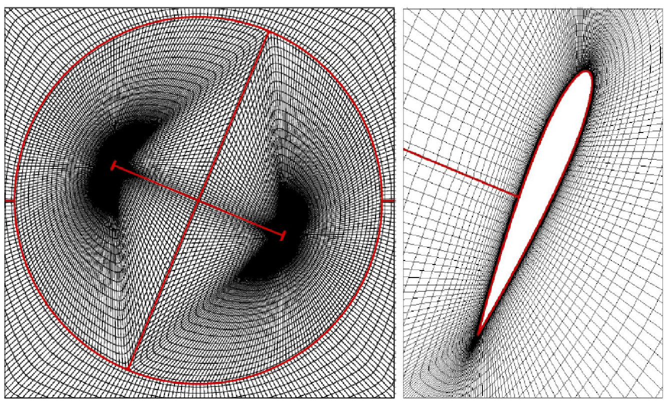

Figure 6: Grid around a wind turbine - Darrieus configuration, Reynolds number 25Âă000

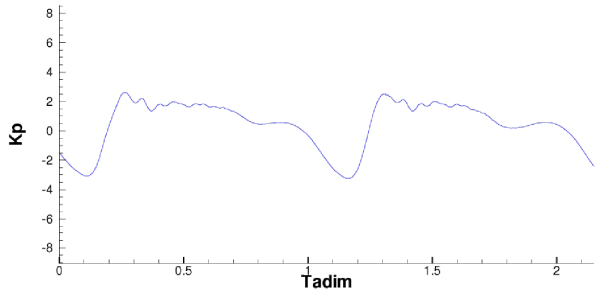

Figure 7: Wind-Turbine gain as a function of timensionless time

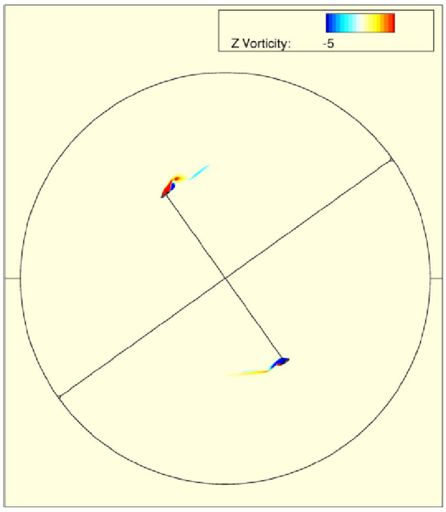

Figure 8: Visualisation of the complete rotor's plan; iso-vorticity field

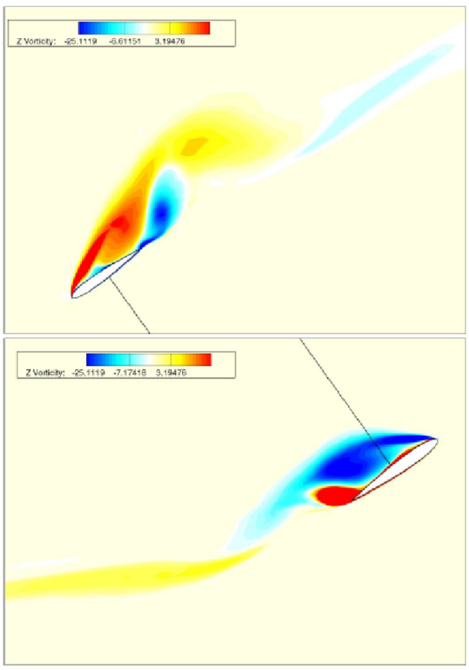

Figure 9: 'Zoom' around the blades. Reduced velocity $(omega * R)/Uupstream = 1.5$. Upstream Reynolds number Re=25000

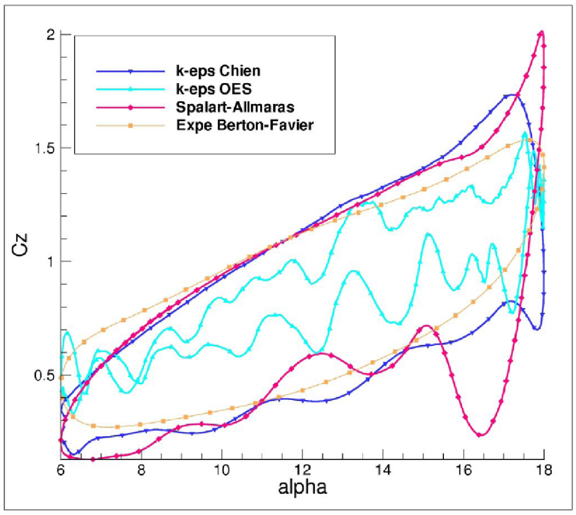

Figure 10: Lift coefficient versus pitch angle around a NACA0012 wing; Reynolds number 100000, mean incidence 12 degrees, oscillation amplitude 6 degrees, position of the oscillation point at 0.25 chord from the leading edge, reduced oscillation frequency 0.188. Experimental test-case by E. Berton, D. Favier, wind-tunnels of Luminy - Marseille, ISM - Institut des Sciences du Mouvement, UMR 7287

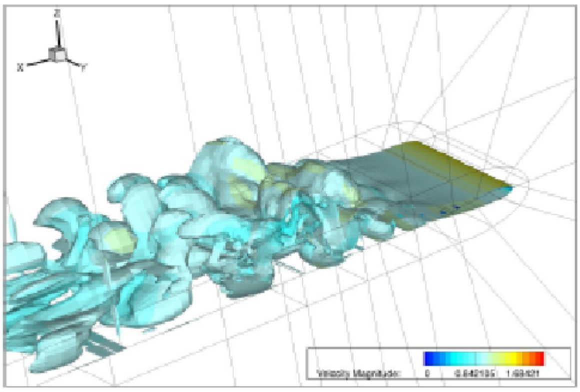

$\alpha = 8^o$ ascendant

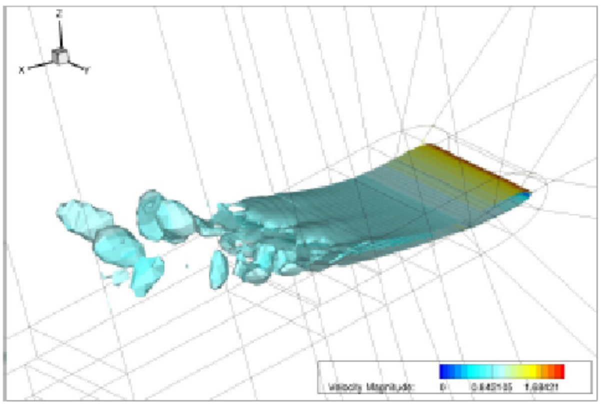

$\alpha = 12^o$ ascendant

Figure 11: Iso-vorticity component perpendicular to the (x,y) plane, pitching flow around the NACA0012 airfoil

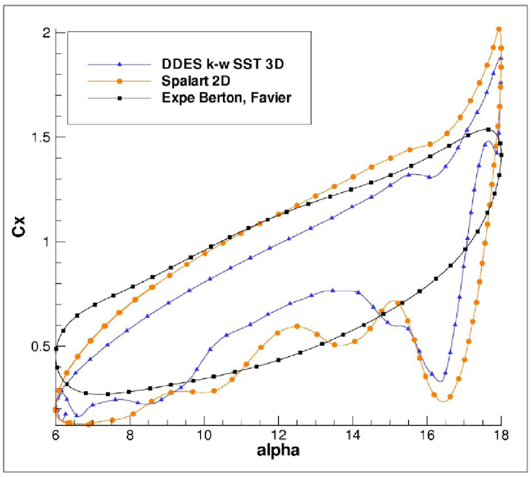

Figure 12: Lift coefficient versus pitching angle of incidence - NACA0012 wing, Re=100000

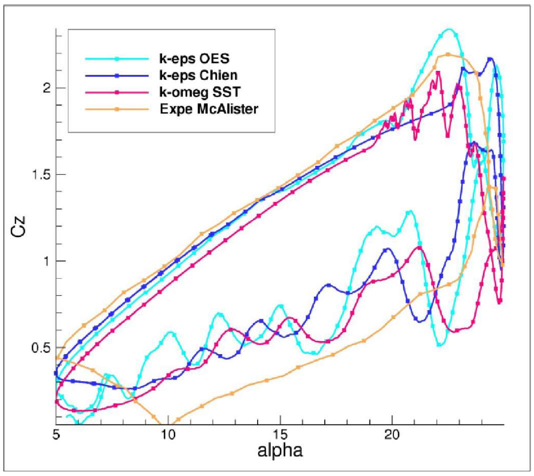

Figure 13: Deep Stall around a pitching NACA0012 wing at Reynolds number of 1 Million, mean incidence of 15 degrees, oscillation amplitude 10 degrees, position of the oscillation at 0.25°$C$from the leading edge, reduced frequency of 0.1. Comparison with the experimental test-case of Mc Alistair et al (1978)

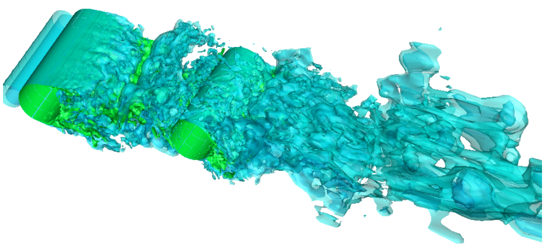

Figure 14: Coherent and turbulent processes capturing by means of the DDES-OES modelling, (Gual-Skopek et al, 2012); IMFT results in the context of the european programme ATAAC, Advanced Turbulence Simulations for Aerodynamic Application Challenges)-FP7, coordinated by DLR-Goettingen

2 Conclusion

The present report is an overview of the IMFT studies carried out about the rotation effects in the near-wall region around bodies, in particular under turbulent flow. Specific turbulence modelling methods have been employed, able to capture non-equilibrium turbulence effects due to the rotation.

References

[1] K.W. McAlister, L.W. Carr and W.J. McCroskey, *Dynamic stall experiments on the NACA0012 airfoil.* TP100, NASA, Technical Paper, 1978

[2] E. Berton, C. Allain, D. Favier and C. Maresca, *Experimental methods for subsonic flow measurements*, Notes on Numerical Fluid Mechanics and Multidisciplinary Design, vol 81, p 251-260, Springer, 2002

[3] M. Gual Skopek, M. Braza, Y. Hoarau, F. Thiele (2012) “Hybrid RANS-LES modelling of a strongly detached turbulent flow around a tandem cylinders configuration“, Series Notes on Numerical Fluid Mechanics and Multidisciplinary Design, Vol. 117.

[3] Braza, M., Perrin, R., Hoarau, Y., 2006. Turbulence properties in the cylinder wake at high reynolds number. J. of Fluid and Struct. 22, 7551–771.

[4] Bourguet, R., Braza, M., Harran, G., El Akoury, R., 2008. Anisotropic organised eddy simulation for the prediction of non-equilibrium turbulent flows around bodies. J. of Fluid and Struct. 24(8), 1240–1251.

[5] Haase, W., Braza, M.,Revell, A., 2009. DESider-A European Effort on Hybrid RANS-LES Modelling. Vol. 103, Notes on Numerical Fluid Mechanics and Multidisciplinary Design, Springer.

[6] J. C. R. Hunt, T. Ishihara, Y. Hoarau, M. Braza, ”Turbulence near interfaces - modelling and simulations“, Key Note Lecture, ERCOFTAC Symposium ”Unsteady Separation in Fluid-Structure Interaction”, 17-21 June 2013, Mykonos, Greece.

[7] S. Mittal. Three-dimensional instabilities in flow past a rotating cylinder. J. Appl.Mech., 71 :89-95, 2004.

[8] G. Martinat, “Analyse physique et modélisation d’écoulements instationnaires turbulents autour de profils oscillants et d’éoliennes ”, PhD Thesis, Institut National Polytechnique de Toulouse, November 2007.

[9] C. Moussaed, S. Wornom, B. Koobus, A. Dervieux, T. Deloze, Y. Hoarau, R. El Akoury, M. Braza, “VMS- and OES-Based Hybrid Simulations of Bluff Body Flows“, ERCOFTAC Symposium ”Unsteady Separation in Fluid-Structure Interaction”, 17-21 June 2013, Mykonos, Greece.

Update on the Study of Flow Around a Rotating Circular Cylinder at a Reynolds Number of 50,000

A. J. Revell[1], S. Rolfo[2] and C. Moulinec [2]

[1] *Modelling & Simulation Centre, University of Manchester, UK*
[2] *STFC Daresbury Laboratory, Scientific Computing Department, UK*

Abstract

As part of an ongoing study, we here report the results of Large Eddy Simulations of the three-dimensional flow around a rotating circular cylinder at a Reynolds number of 5×10^4, with a wall velocity five times the tangential flow velocity. The lift force of a rotating cylinder are known to be considerably higher than those of a regular yacht sail or an aircraft wing of the same projected area, due to the Magnus effect. In recent years there has been something of a renewed interest in this flow.

The primary aim of this work is to build on recent numerical studies of the flow around a rotating smooth cylinder with particular interest in the potential to generate a favourable lift force. Our ongoing objective is be to investigate how this effect can be further enhanced by geometric modifications. In the context of recently awarded access to High Performance Computing facilities provided by the PRACE project [1], a set of wall-resolved Large Eddy Simulations have been undertaken, according to best practice guidelines.

We begin the study with the simulation of the flow around a static cylinder at Re=5×10^4, in which we verify the expected laminar separation mechanism one expects in these conditions. The resolution requirement even to achieve this result are considerable and prevent reliable extension to higher Reynolds number at present. We then apply a rotation rate of $\alpha = \omega R / U_{\text{inf}} = 5$.

Figure 1: A prototype with spanwise discs and a concept with blended diameter [15]

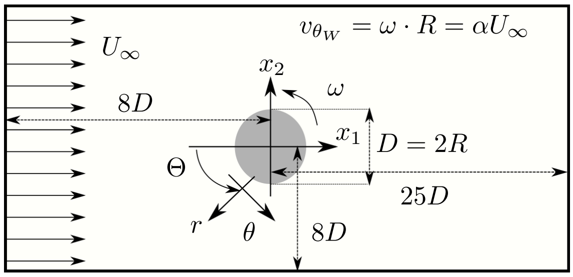

Figure 2: Computational domain

1 Introduction

Following work with Prandtl [13], Flettner demonstrated that large vertical rotating cylinders could be put to use on ships to generate a propulsive force via the Magnus effect. There have since been many studies on this flow, though most have addressed Reynolds numbers far lower than those encountered by Flettner rotors; e.g. Re=200 [12] and Re=300 [6]. However, in order to be of practical use in maritime propulsion, one must consider far higher Reynolds number flow, and the spin ratio α (defined as the ratio between cylinder tangential wall velocity u_{θ_W} and the undisturbed velocity U_∞) is likely to need to be at least in the range 5 - 10. A study by [15] reiterated the potential of Flettner rotors as a viable option for low energy maritime propulsion, and reported two modifications with spanwise discs or 'fences', both flat and with a blended design as shown in Figure 1.

Studies of Flettner rotors with and without discs have been conducted at higher Reynolds numbers using Unsteady Reynolds Averaged Navier-Stokes (URANS) approaches; e.g. 8×10^5 [4] and 5×10^6 [10]. A recent sensitivity study of spanwise disc spacing at moderate Reynolds number by [5] indicated enhancement of the streamwise velocity between the boundary layer of two facing discs. This phenomena, combined with the generation of persistent vortices and a reduction in thickness of the boundary layer around the cylinder itself, acts to increase the lift and reduce the drag (compared to a configuration without span-wise discs). The lack of experimental data for such flow regimes limits the degree of confidence that one can attain, and the predictive accuracy of these results is thus not fully assessed. Furthermore it is difficult to gain insight into the flow physics without some form of turbulent scale resolution.

Indeed the Large Eddy Simulation (LES) study of [3] for flow around a stationary circular cylinder at Re=1.4×10^5 clearly demonstrates the challenges faced by this case even without rotation; a strong dependence was observed on mesh resolution and domain extent, in particular in the span-wise direction. It is perhaps then unsurprising that there is only one instance [9] of the application of LES to the rotating cylinder at high Reynolds number (same as [3]).

The primary objective of the current work is to perform a series of wall-resolved Large Eddy Simulations of

[1] Partnership for Advanced Computing in Europe (www.prace-ri.eu)

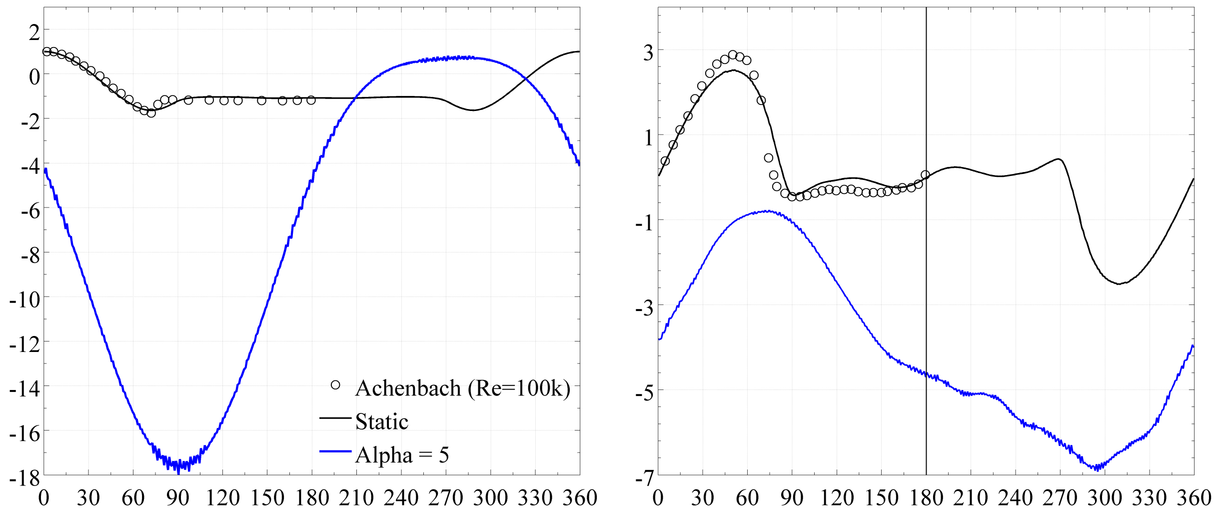

Figure 3: Comparison of the time-averaged values for (left) pressure coefficient $C_P = (P - P_{ref})/(1/2\rho U_{\text{inf}}^2)$ and (right) friction coefficient $C_f = \tau_w/(1/2\rho U_{\text{inf}}^2)$. Numerical results at Re=50,000 are compared to experimental data from [1] at Re=100,000

Table 1: Summary of Results

α	$\overline{C_D}$	C_D'	$\overline{C_L}$	C_L'	$St(C_L)$	θ_{sep}
0	1.01	0.064	0.002	0.36	0.22	84
5	0.45	0.23	-14.42	0.73	0.12	-

the flow around a rotating cylinder at different spin rates up to the representative value of $\alpha = 5$, at a Reynolds of $Re = 5 \times 10^4$. At the spin rate $\alpha = 5$, the flow velocity relative to wall on one side is increased to a local maximum Reynolds of 2.5×10^5.

2 Case Setup & Numerical Details

The domain under consideration is defined in Fig 2 along with relevant dimensions. This is discretised using a two-dimensional mesh of 75×10^3 cells extruded in the spanwise direction using 256 planes; a total of 19.2M cells. The spanwise extent of $Z = 2D$, was deemed to be sufficient in a preliminary work by the authors [14]. The grid has been optimised to ensure sufficient resolution of the near wall physics according to best practise guidelines.

Calculations have been performed using *Code_Saturne* , an open-source CFD code developed by EDF R&D [2], extensively optimised for High Performing Computing as described by [7]. A dynamic procedure has been employed for the evaluation of the Smagorinsky constant [8], with minimization following Lilly [11].

3 Results

Results for the static ($\alpha = 0$) and the rotating case ($\alpha = 5$) have been processed and are summarised in Table 1. For the static case, there are various experimental studies in a similar range of Reynolds, with which one can compare, and broadly there is good agreement. Figure 3 provides the line of the time averaged pressure coefficient C_P and friction coefficient ressure coefficient C_f for both the static, $\alpha = 0$ and the fast rotating, $\alpha = 5$ cases. While the experimental data in Fig 3 are at the higher Reynolds number of 100,000 there is broad agreement. Furthermore, the separation point is here observed to occur before 90°, in line with expectations for this Reynolds number. A drastically altered, asymmetric, flow is observed for the rotating case ($\alpha = 5$), and it can be seen that separation never occurs.

Figures 4 and 5 indicate instantaneous iso-contours of the Q-criterion both cases, at an arbitrary point in the calculation. The contours, set at $Q = 5$ for the static case and $Q = 10$ for the rotating case, are coloured by values of mean pressure, scaled to the maximum values around the cylinder, where blue values indicate low and red high (refer to figure 3 for an indicative scale). In the static case, the laminar separation process can be clearly observed, before transition occurs in the shear layer. For the rotating case, an entirely different flow is observed, whereby pairs of coherent structures persist around the attached side of the cylinder, as previously noted in [14].

Figure 6 provides a snapshot of the ongoing calculation for the case when spanwise discs are added to the cylinder. In this case the geometry is also rotating at $\alpha = 5$.

4 Conclusions

Once completing the validation of the baseline flow around the non-rotating smooth cylinder, we aim to report in detail how the flow changes with rotation, before progressing onwards to examine various geometric configurations, such as a sinusoidally varying diameter and the insertion of discs along the span. Aside from providing physical insight into the lift enhancing mechanisms of these flows, the data from this work is intended to provide a means of validation for more economical turbulence modelling and simulation tools, that one might expect to be used in a more extensive study of the parameter space.

Acknowledgments

The authors gratefully acknowledge PRACE for awarding us access to HERMIT in Germany at The High Performance Computing Center Stuttgart (HLRS). We

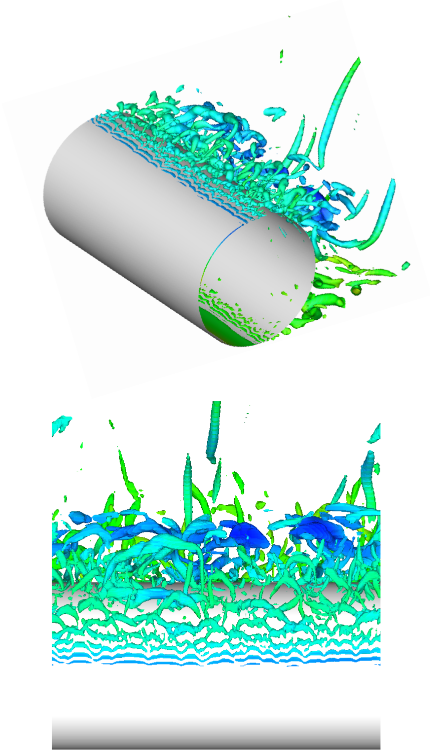

Figure 4: Non rotating case.

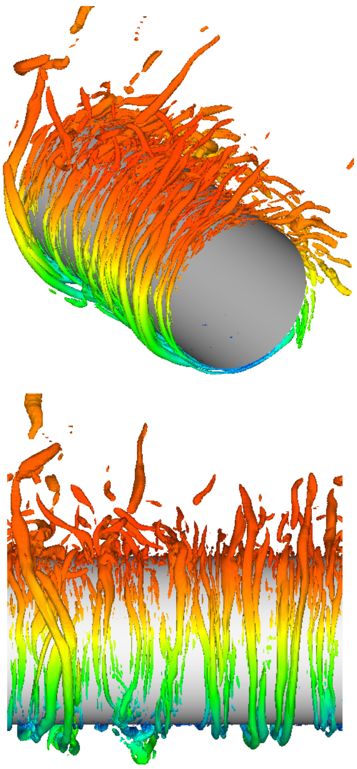

Figure 5: Rotating at $\alpha = 5$.

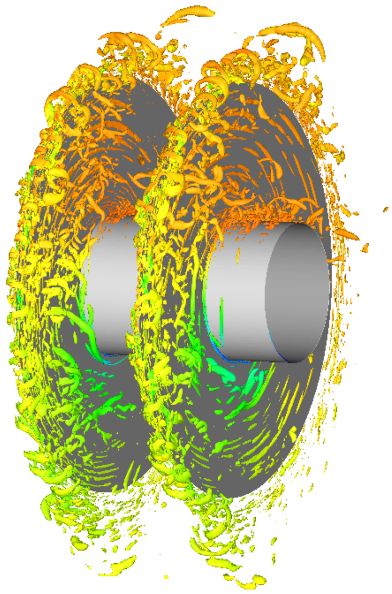

Figure 6: Rotating at $\alpha = 5$ with Spanwise Discs

would also like to thank the UK Engineering and Physical Sciences Research Council (EPSRC) for their support of Collaborative Computational Project 12 (CCP12). We are grateful to Prof. Brian Launder and Dr. Tim Craft for helpful discussions.

5 References

[1] Achenbach, E.: Distribution of local pressure and skin friction around a circular cylinder in cross-flow up to Re= 5×10^6. J. Fluid Mech., **34**, 625-639 (1968)

[2] Archambeau, F., Mechitoua, N., & Sakiz, M.: A finite volume method for the computation of turbulent incompressible flows - industrial applications. Int. J. Finite Volumes, **1**, 1-62 (2004)

[3] Breuer, M.: A challenging test case for large eddy simulation : high Reynolds number circular cylinder flow. Int. J. Heat Fluid Flow, **21**, 648-654 (2000)

[4] Craft, T., Iacovides H., Launder B.: Dynamic performance of Flettner rotors with and without Thom discs. In Proc. 7^{th} Symp. on Turbulence & Shear Flow Phenomena, Ottawa (2011)

[5] Craft, T., Iacovides H., Johnson, N., & Launder B.: Back to the future Flettner-Thom rotors for maritime propulsion ? Turbulence, Heat and Mass Transfer 7 (2012)

[6] El Akoury, R., Braza, M., Perrin, R., Harran, G., Hoarau, Y.: The three-dimensional transition in the flow around a rotating cylinder. J. Fluid Mech., **607**, 0-11 (2008)

[7] Fournier, Y., Bonelle, J., Moulinec, C., Shang, Z., Sunderland, A. G.: Optimizing Code Saturne for Petascale Computations. Comput. Fluids, **45**, 1-12 (2011)

[8] Germano, M., Piomelli, U., Moin, P., Cabot, W. H.: A dynamic subgrid-scale eddy viscosity model. Phys. Fluids A **3**, 1760-1765 (1991)

[9] Karabelas, S. J. . Large Eddy Simulation of high-Reynolds number flow past a rotating cylinder. Int. J. Heat Fluid Flow, **31(4)**, 518-527 (2010)

[10] Karabelas, S. J., Koumroglou, B. C., Argyropoulos, C. D., Markatos, N. C. (2012). c. Applied Mathematical Modelling, **36(1)**, 379-398 (2012)

[11] Lilly, D. K.: A proposed modification of the Germano subgrid-scale closure method. Phys. Fluids A, **4(3)**, 633 (1992)

[12] Mittal, S., Kumar, B.: Flow past a rotating cylinder. J. Fluid Mech., **76**. (2003)

[13] Prandtl, L.: The Magnus effect and wind-powered ships. Naturwissenschaften, **13**, (1925)

[14] Rolfo, S., Revell, A. : DESider - Effect of span-wise resolution for LES of flow over a rotating cylinder at high Reynolds. DLES9 (2013)

[15] Salter, S., Sortino G., Latham J.: Seagoing hardware for the cloud albedo method of reversing global warming. Philos. Trans.: Math., Phys. Eng. Sci., **366**, 3989-4006 (2008)

ERCOFTAC Workshops and Summer Schools

ERCOFTAC Workshops, Conferences - 2014

Title	Location	Date	Coordinators	Organiser
EPSRC-ERCOFTAC Workshop Turbulent flows generated/designed in multiscale/fractal ways: fundamentals and applications	London, UK	26-27/03/2014	Laizet, S. Vassilicos, Ch	SIG44, Co: EPSRC
Recent progress in triadic closures and wave turbulence theory	Paris, France	05-06/05/2014	Sagaut, P.	SIG35, Co: Henri Benard PC
Progress in Wall Turbulence: Understanding and Modelling	Villenuve d'Ascq, France	18-20/06/2014	Stanislas, M.	SIG15
Synthetic turbulence, wavelet and CFD	Nuremberg, Germany	30/06-01/07/2014	Delgado, A.	SIG42
IMA7 - 7th Conference of the International Marangoni Association	Vienna,Austria	23-26/06/2014	Kuhlmann, H.	PC Alpe-Danube-Adria

ERCOFTAC Summer Schools, Courses - 2014

Title	Location	Date	Coordinators	Organiser
New Challenges in Turbulence Research III (http://NCTR.EU)	Les Houches, France	16-21/03/2014	Gibert, M.	PC Henri Benard SIG35
SIG12/SIG43/FP1005 training school on "Collective dynamics of particles: from viscous to turbulent flows"	Udine, Italy	26-30/05/ 2014	Marchioli, C.	SIG12 SIG43
Cavitation instabilities and rotordynamic effects in turbopumps and hydroturbines	Udine, Italy	7-11/06/2014	d'Agostino, L. Salvetti, M. V.	SIG12 Co: CISM

Programme of Events 2014

Dr. Richard E. Seoud

Open for Registration ⟹ `richard.seoud-ieo@ercoftac.org`

CFD for Dispersed Multi-Phase Flows,IV

3-4 April 2014, GE, Munich, Germany
Fees: Members € 594, Non-members € 995
Course Coordinator: Prof. Martin Sommerfeld, University Halle-Wittenberg, Germany

The simultaneous presence of several different phases in external or internal flows such asgas, liquid and solid is found in daily life, environment and numerous industrial processes. These types of flows are termed multiphase flows, which may exist in different forms depending on the phase distribution. Examples are gas-liquid transportation, crude oil recovery, circulating fluidized beds, sediment transport in rivers, pollutant transport in the atmosphere, cloud formation, fuel injection in engines, bubble column reactors and spray for food processing, to name only a few. As a result of the interaction between the different phases such flows are rather complicated and very difficult to describe theoretically. For the design and optimisation of such multiphase systems a detailed understanding of the interfacial transport phenomena is essential. This course is rather unique as it is one of few in the community that is specifically designed to deliver,a) abest practice guidance and b) the latest trends, in CFD for dispersed multi-phase flows.

The course appeals to researchers and engineers involved in projects requiring CFD for (wall-bounded) turbulent dispersed multiphase flows with bubbles, drops or particles. Moreover, delegates are offered the opportunity to present their work via 10 minute presentations, thereafter, the lecturers can offer prospective solution.

Computational Aeroacoustics, II

9-10 October 2014, GE, Munich, Germany
Fees: Members € 640, Non-members € 995
Course Coordinator: Prof. Christophe Bailly, EC Lyons, France

9-10 October 2014, GE, Munich, Germany Fees: Members 640, Non-members 995 Course Coordinator: Prof. Christophe Bailly, EC Lyons, France This course is intended for researchers in industry and in academia including Ph.D. Students with a good knowledge in fluid mechanics, who would like to build up or widen their knowledge in the field of aeroacoustics (modeling, computational tools and industrial applications). It will first provide a comprehensive overview of recent insights of aeroacoustics theories (Lighthills analogy and vortex sound theory, extensive hybrid approaches and wave extrapolation methods, duct acoustics). A number of practical problems involving the coupling between CFDs results and CAA will be also thoroughly discussed (e.g. how design a mesh size for aeroacoustics applications using large eddy simulation, inclusion of mean flow effects via hybrid formulations such as the acoustic perturbation equations, presence of surfaces, aeroacoustic couplings,) and realistic applications performed by the instructors (aeronautics, car industry, propulsion, energy,) will be discussed. Advanced computational aeroacoustics methods will be also presented as well as what we can learn from the direct computation of aerodynamic noise. Finally, specific topics reflecting participant interests will be discussed in a final round table session.

Fluid Structure Interaction with Impact on Industrial Applications

16-17 October 2014, EDF, Chatou-Paris, France
Fees: Members € 540, Non-Members € 875
Course Coordinator: Dr. Marianna Braza, IMFT, France, & Dr. Elisabeth Longatte, EDF, France

The scope of this course is to bring together the academic and industrial scientific communities in Fluid Dynamics (FD) and Structural Mechanics (SM) on this topic, in order to address the state-of-the-art methods in theoretical, experimental and numerical approaches. The course contents involve fluid-structure interaction phenomena associated with solid structure rotation, fluid-structure coupling involving instabilities, vibrations, separation. A principal goal is to enable researchers in the FSI community with state-of-the-art methods for analysing the fluid-structure interaction phenomena and to come up with quality achievements and best practice guidelines for efficient and secure design. The domains of applications cover a large spectrum including flow and movement induced vibrations in hydrodynamics and in aerodynamics. The course will be composed of ten Key Note Lectures. A large audience coming from the above academic and industrial communities is previewed.

Mathematical Methods and Tools in Uncertainty Management and Quantification IV

4-5 November 2014, AREVA, La Defense, Paris, France
Fees: Members: €640, Non- Members: €995
Course Coordinator: Prof. Charles Hirsch,Em. Vrije Universiteit Brussel, Pres. Numeca Int'l, Belgium

Uncertainty quantification is a new paradigm in industrial analysis and design as it aims at taking into account the presence of numerous uncertainties affecting the behaviour of physical systems. Dominating uncertainties can be either be operational (such as boundary conditions) and//or geometrical resulting from unknown properties, such as tip clearances of rotating fan blades or from manufacturing tolerances. Other uncertainties are related to models, such as turbulence or combustion should also be considered, or to numerical related errors. Whether bringing a new product from conception into production or operating complex plant and production processes , commercial success rests on careful management and control of risk in the face of many interacting uncertainties. Historically, chief engineers and project managers have estimated and managed risk using mostly human judgment founded upon years of experience and heritage. As the 21st century begins to unfold, the design and engineering of products as well as the control of plant and process are increasingly relying on computer models and simulation. This era of virtual design and prototyping opens the opportunity to deal with uncertainty in a systematic formal way by which sensitivities to various uncertainties can be quantified and understood, and designs and processes optimized so as to be robust against such uncertainties.

After several successful Courses on the applications of UQ, ERCOFTAC decided, based on requests from many participants, to focus the present Course on the mathematical methodologies of UQ, enabling the participants to develop an in-depth understanding of the main methods such as: spectral, including polynomial chaos methods; methods of moments and Monte-Carlo methodologies. The lectures will be given by worldwide recognised experts in these fields, who will cover the basics as well as representative applications.

Best Practice For Engineering CFD III (3rd delivery)

26-27 November, 2014, CMT-Motores Trmicos, Valencia, SPAIN
Fees: Members €640, Non- Members €995
Course Coordinator: Prof. Charles Hirsch,Em. Vrije Universiteit Brussel, Pres. Numeca Int'l, Belgium

This course is targeted atrelatively new and improving CFD analysts in engineering industries and consultancies. It providesthe knowledgeto effect a step-change in the accuracy and reliability of CFD practices across a range of engineering applications relevant to the power generation, aerospace, automotive, built environment and turbomachinery sectors amongst others. This course is directly relevant to engineering applications of CFD for single-phase, compressible and incompressible, steady and unsteady,turbulent flows, with and without heat transfer. Much of the content will also be relevant to even more complex engineering applications. The main focus will be on RANS applications, but an introduction to the special considerations required by LES and hybrid methods is also given. The course provides the means for CFD analysts to significantly enhance their use of commercial and open-source CFD software for engineering applications. In particular, it provides guidance on best practices and highlights common pitfalls to be avoided.

ERCOFTAC / SIG 42

10th Conference on Synthetic Turbulence Models

Synthetic turbulence, wavelet and CFD

4th and 5th September 2014, Erlangen, Germany
LSTM University of Erlangen-Nuremberg, Germany

Organisers
A. Delgado, LSTM University of Erlangen-Nuremberg, Germany
Long Zhou, LSTM University of Erlangen-Nuremberg, Germany
F. Nicolleau, University of Sheffield, UK
T. Michelitsch, Université Pierre et Marie Curie, France
A. Nowakowski, University of Sheffield, UK

Website
http://www.sig42.group.shef.ac.uk/SIG42-10.htm

Audience

This conference on synthetic turbulence organised by ERCOFTAC/SIG 42 is open to anyone interested in flow modeling and/or "synthetic turbulence" including (but not restricted to) Kinematic Simulation (KS). More fundamental talks on particle dispersion in turbulent flows or fluid dynamics are also welcome.

Motivation

KS is widely used in various domains, including Lagrangian aspects in turbulence mixing/stirring, particle dispersion/clustering, and last but not least, aeroacoustics. Flow realisations with complete spatial, and sometime spatio-temporal, dependency, are generated via superposition of random modes (mostly spatial, and sometime spatial and temporal, Fourier modes), with prescribed constraints such as: strict incompressibility (divergence-free velocity field at each point), high Reynolds energy spectrum. Recent improvements consisted in incorporating linear dynamics, for instance in rotating and/or stably-stratified flows, with possible easy generalisation to MHD flows, and perhaps to plasmas. KS for channel flows have also been validated. However, the absence of "sweeping effects" in present conventional KS versions is identified as a major drawback in very different applications: inertial particle clustering as well as in aeroacoustics. Nevertheless, this issue was addressed in some reference papers, and merits to be revisited in the light of new studies in progress. A further goal of this conference is to bring people from different disciplines together. In particular recent emerging fractal approaches have the potential to provide the framework for the construction of new synthetic turbulent flows. Interdisciplinary contributors are especially invited to contribute.

Related topics

Synthetic models of turbulence (KS and others), Lagrangian aspects of turbulence, vortex dynamics and structure formation, particle dispersion/clustering, vorticity and multiphase flows, vortex methods, DNS/LES and related techniques, turbulent flows and multiscale (fractal) shapes

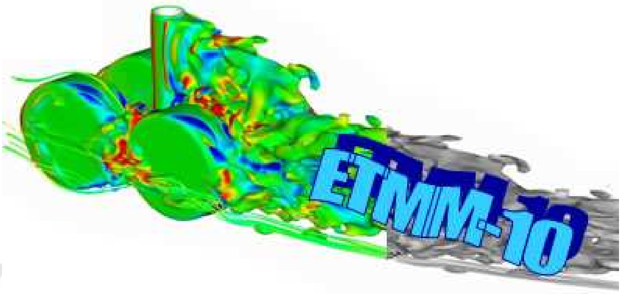

ETMM 10

10th International ERCOFTAC Symposium on Engineering Turbulence Modelling and Measurements

17 - 19 September 2014
Don Carlos Resort, Marbella, Spain

Symposium website: www.etmm10.info

Organizers
Prof. Michael Leschziner, Chairman, Imperial College
Prof. Wolfgang Rodi, Co-chairman, Karlsruhe Institute of Technology
The ETMM Series of Conferences

Aims

The ETMM series of symposia aims to provide a bridge between researchers and practitioners in Flow,Turbulence and Combustion by reporting progress in the predominantly applied, industrially-oriented areas of turbulence research.This includes the development, improvement and application of statistical closures, simulation methods and experimental techniques for complex flow conditions that are relevant to engineering practice; the modelling of interactions between turbulence and chemistry, dispersed phases and solid structures; and the symbiosis of modelling, simulation and experimental research.

Major Themes

- Novel modelling and simulation methods for practically relevant turbulent flows, including interaction with heat and mass transfer, rotation, combustion and multi-phase transport
- Novel experimental techniques for flow, turbulence and combustion and new experimental studies and data sets
- Innovative applications of modelling, simulation and experimental techniques to complex flows, industrial configurations and optimisation problems
- High-speed aerodynamics, acoustics and flow control with emphasis on turbulence processes
- Modelling, simulation and measurements of environmental and bio-spherical flows

Abstracts are invited for submission by **15th January 2014**, via the Symposium Website.
Final manuscripts and updated abstracts are due by **1st July 2014**.

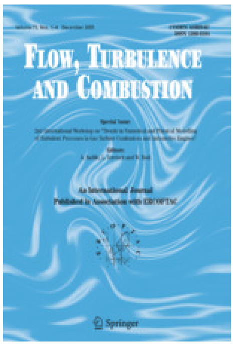

RECENT TABLE OF CONTENTS OF FLOW TURBULENCE AND COMBUSTION

AN INTERNATIONAL JOURNAL PUBLISHED BY SPRINGER
IN ASSOCIATION WITH ERCOFTAC

EDITOR-IN-CHIEF: K. HANJALIĆ
EDITORS: J.J. CHEN, M. REEKS, W. RODI, L. VERVISCH
HONORARY EDITOR: J.C.R HUNT
FOUNDING EDITOR: F. NIEUWSTADT

VOLUME 92, NUMBER 1-2, JANUARY 2014

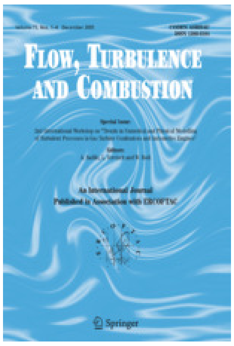

RECENT TABLE OF CONTENTS OF FLOW TURBULENCE AND COMBUSTION

AN INTERNATIONAL JOURNAL PUBLISHED BY SPRINGER
IN ASSOCIATION WITH ERCOFTAC

VOLUME 92, NUMBER 3, MARCH 2014

Further articles can be found at `www.springerlink.com`

Abstracted/Indexed in Science Citation Index, Science Citation Index Expanded (SciSearch), Journal Citation Reports/Science Edition, SCOPUS, INSPEC, Chemical Abstracts Service (CAS), Google Scholar, EBSCO, CSA, ProQuest, Academic OneFile, ASFA, Current Abstracts, Current Contents/Engineering, Computing and Technology, Earthquake Engineering Abstracts, EI Encompass, Ei Page One, EI-Compendex, EnCompassLit, Engineered Materials Abstracts, Gale, OCLC, PASCAL, SCImago, STMA-Z, Summon by Serial Solutions, VINITI - Russian Academy of Science.

Instructions for Authors for Flow Turbulence Combust are available at `http://www.springer.com/10494`.

ERCOFTAC Special Interest Groups

1. **Large Eddy Simulation**
Geurts, B.J.
University of Twente, Holland.
Tel: +31 534 894 125
b.j.geurts@utwente.nl

4. **Turbulence in Compressible Flows**
Dussauge, Jean-Paul
IUSTI, Marseille
jean-paul.dussauge
@polytech.univmrs.fr

5. **Environmental Fluid Mechanics**
Armenio, V.
Universit di Trieste, Italy.
Tel: +39 040 558 3472
Fax: +39 040 572 082
armenio@dica.units.it

10. **Transition Modelling**
Dick, E.,
University of Ghent, Belgium.
Tel: +32 926 433 01
Fax: +32 926 435 86
erik.dick@ugent.be

12. **Dispersed Turbulent Two Phase Flows**
Sommerfeld, M.
Martin-Luther University, Germany.
Tel: +49 346 146 2879
Fax: +49 346 146 2878
martin.sommerfeld@iw.uni-halle.de

14. **Stably Stratified and Rotating Flows**
Redondo, J.M.
UPC, Spain.
Tel: +34 934 017 984
Fax: +34 934 016 090
redondo@fa.upc.edu

15. **Turbulence Modelling**
Jakirlic, S.
Darmstadt University of Technology, Germany.
Tel: +49 615 116 3554
Fax: +49 615 116 4754
s.jakirlic@sla.tu-darmstadt.de

20. **Drag Reduction and Flow Control**
Choi, K-S.
University of Nottingham, England.
Tel: +44 115 951 3792
Fax: +44 115 951 3800
kwing-so.choi@nottingham.ac.uk

24. **Variable Density Turbulent Flows**
Anselmet, F.
IMST, France.
Tel: +33 491 505 439
Fax: +33 491 081 637
anselmet@irphe.univ-mrs.fr

28. **Reactive Flows**
Angelberger, C.
IFP Energies Nouvelles, France
Tel: +33 147 527 420
christian.angelberger@ifpen.fr

32. **Particle Image Velocimetry**
Stanislas, M.
Ecole Centrale de Lille, France.
Tel: +33 320 337 170
Fax: +33 320 337 169
Michel.Stanislas@ec-lille.fr

33. **Transition Mechanisms, Prediction and Control**
Hanifi, A.
FOI, Sweden.
Tel: +46 855 503 197
Fax: +46 855 503 397
ardeshir.hanifi@foi.se

34. **Design Optimisation**
Giannakoglou, K.
NTUA, Greece.
Tel: +30 210 772 1636
Fax: +30 210 772 3789
kgianna@central.ntua.gr

35. **Multipoint Turbulence Structure and Modelling**
Cambon, C.
ECL Ecully, France.
Tel: +33 472 186 161
Fax: +33 478 647 145
claude.cambon@ec-lyon.fr

36. **Swirling Flows**
Braza, M.
IMFT, France.
Tel: +33 534 322 839
Fax: +33 534 322 992
braza@imft.fr

37. **Bio-Fluid Mechanics**
Poelma, C.
Delft University of Technology, Holland.
Tel: +31 152 782 620
Fax: +31 152 782 947
c.poelma@tudelft.nl

38. **Micro-thermofluidics**
Borhani, N.
EPFL, Switzerland.
Tel: +41 216 933 503
Fax: +41 216 935 960
navid.borhani@epfl.ch

39. **Aeroacoustics**
Bailly, C.
Ecole Centrale de Lyon, France.
Tel: +33 472 186 014
Fax: +33 472 189 143
christophe.bailly@ec-lyon.fr

40. **Smoothed Particle Hydrodynamics**
Le Touze, D.
Ecole Centrale de Nantes, France
Tel: +33 240 371 512
Fax: +33 240 372 523
David.LeTouze@ec-nantes.fr

41. **Fluid Structure Interaction**
Longatte, E.
EDF, France.
Tel: +33 130 878 087
Fax: +33 130 877 727
elisabeth.longatte@edf.fr

42. **Synthetic Models in Turbulence**
Nicolleau, F.
University of Sheffield, England.
Tel: +44 114 222 7867
Fax: +44 114 222 7890
f.nicolleau@sheffield.ac.uk

43. **Fibre Suspension Flows**
Lundell, F.
The Royal Institute of Technology, Sweden.
Tel: +46 87 906 875
frederik@mech.kth.se

44. **Fundamentals and Applications of Fractal Turbulence**
Fortune, V.
Universit de Poitiers, France.
Tel: +33 549 454 044
Fax: +33 549 453 663
veronique.fortune@lea.univ-poitiers.fr

45. **Uncertainty Quantification in Industrial Analysis and Design**
Meyers, J.
Katholieke Universiteit Leuven, Belgium.
Tel: +32 163 225 02
Fax: +32 163 229 85
johan.meyers@mech.kuleuven.be

ERCOFTAC Pilot Centres

Alpe - Danube - Adria
Gergely, K.
Department of Fluid Mechanics,
Budapest University of Technology and Economics
Bertalan L. utca 4-6
1111 Budapest, Hungary
Tel: +36 1 463 4073
Fax: +36 1 463 4072
kristof@ara.bme.hu

Belgium
Geuzaine, P.
Cenaero,
CFD Multi-physics Group,
Rue des Fréres Wright 29,
B-6041 Gosselies,
Belgium.
Tel: +32 71 919 334
philippe.geuzaine@cenaero.be

Brasil
Rodriguez, O.
Department of Mechanical Engineering,
Sao Carlos School of Mechanical Engineering,
Universidade de Sao Paulo,
Brasil.
oscarmhr@sc.usp.br

Czech Republic
Bodnar, T.
Institute of Thermomechanics AS CR,
5 Dolejskova,
CZ-18200 Praha 8,
Czech Republic.
Tel: +420 224 357 548
Fax: +420 224 920 677
bodnar@marian.fsik.cvut.cz

France - Henri Bénard
Cambon, C.
Ecole Centrale de Lyon.
LMFA, B.P. 163,
F-69131 Ecully Cedex,
France.
Tel: +33 4 72 18 6161
Fax: +33 4 78 64 7145
claude.cambon@ec-lyon.fr

France South
Braza, M.
IMF Toulouse,
CNRS UMR - 5502,
Allée du Prof. Camille Soula 1,
F-31400 Toulouse Cedex, France.
Tel: +33 534 322 839
Fax: +33 534 322 992
Braza@imft.fr

France West
Danaila, L.
CORIA, University of Rouen,
Avenue de l'Université BP12,
76801 Saint Etienne du Rouvray
France.
Tel: +33 232 953 702
luminita.danaila@coria.fr

Germany North
Gauger, N.R.
Computational Mathematics Group
RWTH Aachen University
Schinkelstr. 2
D-52062 Aachen, Germany
Tel: +49 241 80 98 660
Fax: +49 241 80 92 600
gauger@mathcces.rwth-aachen.de

Germany South
Becker, S.
Universität Erlangen, IPAT
Cauerstr. 4
91058 Erlangen
Germany
Tel: +49 9131 85 29451
Fax: +49 9131 85 29449
sb@ipat.uni-erlangen.de

Greece
M. Founti.
National Tech. University Of Athens,
School of Mechanical Engineering,
Lab. of Steam Boilers and Thermal Plants,
Heroon Polytechniou 9,
15780 Zografou, Athens, Greece
Tel: +30 210 772 3605
Fax: +30 210 772 3663
mfou@central.ntua.gr

Iberian East
Onate, E.
Universitat Politecnica de Catalunya,
Edificio C-1, Campus Norte,
Gran Capitan s/n,
E-08034 Barcelona,
Spain.
Tel: +34 93 401 6035
Fax: +34 93 401 6517
onate@cimne.upc.es

Iberian West
Theofilis, V.
Research Professor of Fluid Mechanics
School of Aerospace Engineering
Technical University of Madrid (UPM)
Tel: +34 91 336 3298
Fax: +34 91 336 3295
vassilios.theofilis@upm.es

Italy
Rispoli, F.
Tel: +39 064 458 5233
franco.rispoli@uniroma1.it
Borello, D
Tel: +39 064 458 5263
domenico.borello@uniroma1.it
Sapienza University of Rome,
Via Eudossiana, 18
00184 Roma, Italy

Netherlands
Ooms, G.
J.M. Burgerscentrum,
National Research School for Fluid Mechanics,
Mekelweg 2,
NL-2628 CD Delft, Netherlands.
Tel: +31 15 278 1176
Fax: +31 15 278 2979
g.ooms@tudelft.nl

Nordic
Wallin, S.
Swedish Defence Research Agency FOI,
Information and Aeronautical Systems,
S-16490 Stockholm,
Sweden.
Tel: +46 8 5550 3184
Fax: +46 8 5550 3062
stefan.wallin@foi.se

Poland
Rokicki, J.
Warsaw University of Technology,
Inst. of Aeronautics & Applied Mechanics,
ul. Nowowiejska 24,
PL-00665 Warsaw, Poland.
Tel: +48 22 234 7444
Fax: +48 22 622 0901
jack@meil.pw.edu.pl

Switzerland
Jenny, P.
ETH Zürich,
Institute of Fluid Dynamics,
Sonneggstrasse 3,
8092 Zürich, Switzerland.
Tel: +41 44 632 6987
jenny@ifd.mavt.ethz.ch

United Kingdom
Standingford, D.
Zenotech Ltd.
University Gate East, Park Row,
Bristol, BS1 5UB
England.
Tel: +44 117 302 8251
Fax: +44 117 302 8007
david.standingford@zenotech.com

Best Practice Guidelines for Computational Fluid Dynamics of Dispersed Multi-Phase Flows

Editors

Martin Sommerfeld, Berend van Wachem
&
René Oliemans

The simultaneous presence of several different phases in external or internal flows such as gas, liquid and solid is found in daily life, environment and numerous industrial processes. These types of flows are termed multiphase flows, which may exist in different forms depending on the phase distribution. Examples are gas-liquid transportation, crude oil recovery, circulating fluidized beds, sediment transport in rivers, pollutant transport in the atmosphere, cloud formation, fuel injection in engines, bubble column reactors and spray driers for food processing, to name only a few. As a result of the interaction between the different phases such flows are rather complicated and very difficult to describe theoretically. For the design and optimisation of such multiphase systems a detailed understanding of the interfacial transport phenomena is essential. For single-phase flows Computational Fluid Dynamics (CFD) has already a long history and it is nowadays standard in the development of air-planes and cars using different commercially available CFD-tools.

Due to the complex physics involved in multiphase flow the application of CFD in this area is rather young. These guidelines give a survey of the different methods being used for the numerical calculation of turbulent dispersed multiphase flows. The Best Practice Guideline (BPG) on Computational Dispersed Multiphase Flows is a follow-up of the previous ERCOFTAC BPG for Industrial CFD and should be used in combination with it. The potential users are researchers and engineers involved in projects requiring CFD of (wall-bounded) turbulent dispersed multiphase flows with bubbles, drops or particles.

Table of Contents

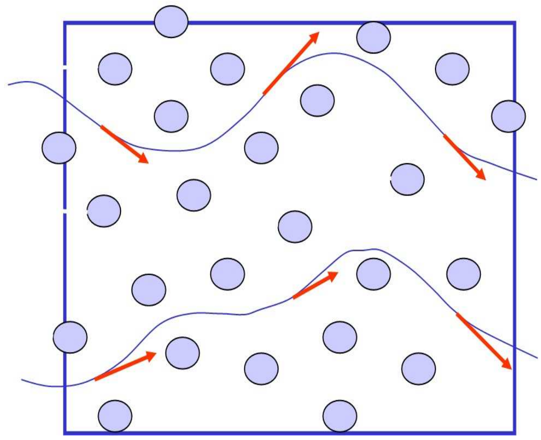

Copies of the Best Practice Guidelines can be acquired electronically from the ERCOFTAC website:

www.ercoftac.org

Or from:

ERCOFTAC CADO
Crown House
72 Hammersmith Road
London W14 8TH, United Kingdom

Tel: +44 207 559 1429
Fax: +44 207 559 1428
Email: magdalena.jakubczak@ercoftac.org

The price per copy (not including postage) is:

ERCOFTAC members	
First copy	*Free*
Subsequent copies	75 Euros
Students	75 Euros
Non-ERCOFTAC academics	140 Euros
Non-ERCOFTAC industrial	230 Euros
EU/Non EU postage fee	10/17 Euros